TITLE

Upregulated GIRK2 counteracts ethanol-induced changes in excitability and respiration in human neurons

AUTHORS

Iya Prytkova[1], Yiyuan Liu[2], Michael Fernando[1], Isabel Gameiro-Ros[1], Dina Popova[3], Chella Kamarajan[4], Xiaoling Xuei[5], David B. Chorlian[4], Howard J. Edenberg[5,6], Jay A. Tischfield[3], Bernice Porjesz[4], Zhiping P. Pang[3,7], Ronald P. Hart[3,8], Alison Goate[1,2,] *, and Paul A. Slesinger[1,] *

[1]Nash Family Department of Neuroscience, Icahn School of Medicine at Mount Sinai, New York, NY 10029
[2]Department of Genetics & Genomic Sciences, Icahn School of Medicine at Mount Sinai, New York, NY 10029
[3]Human Genetics Institute, Rutgers University, Piscataway, NJ 08854
[4]Dept. of Psychiatry & Behavioral Sciences, SUNY Downstate Health Sciences University, Brooklyn, NY 11203
[5]Department of Medical and Molecular Genetics, Indiana University School of Medicine, Indianapolis, IN 46202
[6]Department of Biochemistry and Molecular Biology, Indiana Univ School of Medicine, Indianapolis, IN 46202
[7]Department of Neuroscience and Cell Biology and The Child Health Institute of New Jersey, Rutgers Robert Wood Johnson Medical School, New Brunswick, NJ, 08901
[8]Department of Cell Biology & Neuroscience, Rutgers University, Piscataway, NJ 08854

*Corresponding authors

Contact information:

Alison Goate: alison.goate@mssm.edu

Paul Slesinger: paul.slesinger@mssm.edu

SUMMARY

Genome-wide association analysis of electroencephalographic endophenotypes for alcohol use disorder has identified non-coding polymorphisms within the *KCNJ6* gene. *KCNJ6* encodes the GIRK2 protein, a subunit of a G-protein-coupled inwardly-rectifying potassium channel that regulates neuronal excitability. To elucidate how GIRK2 affects neuronal excitability and the response to ethanol exposure, we upregulated *KCNJ6* in human glutamatergic neurons derived from induced pluripotent stem cells using two distinct strategies: CRISPRa induction and lentiviral expression. Multi-electrode-arrays, calcium imaging, patch-clamp electrophysiology, and mitochondrial stress tests collectively show that elevated GIRK2 acts in concert with 7-21 days of ethanol exposure to inhibit neuronal activity, to counteract ethanol-induced increases in glutamate sensitivity, and to promote an increase intrinsic excitability. Furthermore, ethanol exposure did not alter basal nor activity-dependent mitochondrial respiration in elevated GIRK2 neurons. These data highlight a role for GIRK2 in mitigating the effects of ethanol on neuronal glutamatergic signaling and mitochondrial activity.

Key Words: Alcohol, *KCNJ6*, hiPSC, CRISPRa, glutamate, excitability, mitochondria

Graphical Abstract:

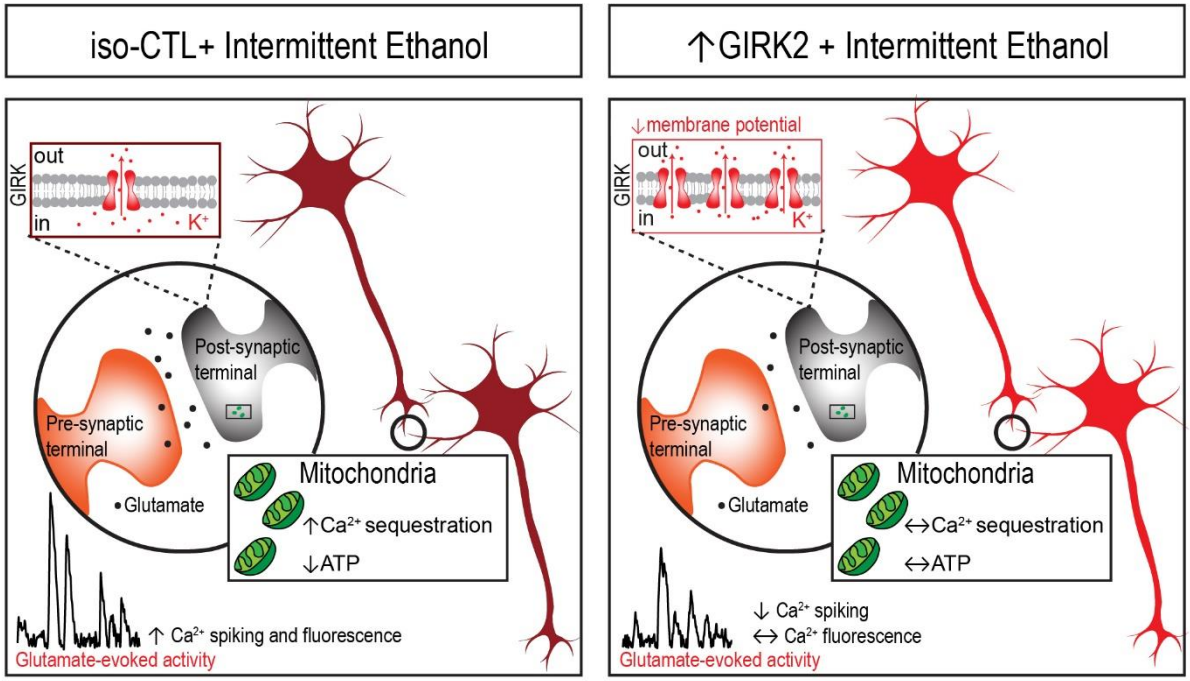

INTRODUCTION

A genome wide association study (GWAS) conducted by the Collaborative Study on the Genetics of Alcoholism (COGA) identified single nucleotide polymorphisms (SNPs) in the *KCNJ6* gene associated with variations of electroencephalogram (EEG) frontal theta event-related oscillations (θ-EROs) to task-relevant target stimuli during a visual oddball task[1]. Furthermore, *KCNJ6* SNPs have been linked to frontal θ-EROs during other tasks evaluating attention, inhibitory control, and reward processing, in addition to influencing neurodevelopmental trajectories during adolescence and young adulthood with age- and sex-specific effects[1–3]. Low frontal θ-ERO during these tasks is characteristic of individuals with alcohol use disorder (AUD) as well as their high-risk offspring and considered to be an endophenotype for (AUD)[4,5]. Most of the associated *KCNJ6* SNPs are non-coding, with the exception of a single imputed synonymous SNP, and therefore are expected to primarily impact gene expression, which was recently shown with human neurons containing different *KCNJ6* SNPs[1,6].

KCNJ6 encodes a G protein-coupled inwardly-rectifying potassium channel subunit 2, GIRK2 (Kir3.2), which plays a key role in controlling neuronal excitability[7,8]. In humans, GIRK2 is largely present as a homotetramer or in a heterotetramer with GIRK1 (Kir3.1)[8]. The channel is coupled to $G_{i/o}$ G-protein coupled receptors (GPCRs), including γ-aminobutyric acid receptor $GABA_B$, dopamine receptor D_2R, Group II metabotropic glutamate receptors (mGluRs), serotonin receptor 5-HT_{1a}, and cannabinoid receptor CB_1[8]. Ligand-binding and subsequent dissociation of the G-protein trimer leads to GIRK activation by Gβγ, outward potassium flux, and inhibition of neuronal firing[8,9]. Importantly, alcohol can directly activate GIRK2 via interaction with a hydrophobic pocket in the cytoplasmic domain[9–11]. In addition to these direct activation mechanisms, GIRK channels also depend on phosphatidylinositol 4,5-biphosphate (PIP_2)-binding and membrane cholesterol to facilitate conformational changes underlying channel activation[9,12]. Studies in mice have shown that GIRK2 affects reward mechanisms and behaviors associated with alcohol as well as other drugs of abuse[13–15]. The channel is broadly expressed throughout the brain in multiple neuronal cell types, including cortical pyramidal neurons[16]. Thus, it is possible that differences in GIRK2 expression can contribute to changes in neuronal excitability and thus influence the EEG θ-EROs.

However, the direct impact of changes in GIRK2 expression on human neuronal physiology remains poorly understood. To better understand the effect of GIRK2 levels independently of other genetic factors, such as differences in genetic strain, we manipulated the expression of GIRK2 either through CRISPRa[17] or with a lentiviral vector in neurons derived from healthy donors, thus enabling a comparison of upregulated

GIRK2 in the same cell line (i.e., isogenic). We hypothesized that elevated GIRK2 expression would influence neuronal activity and adaptations to ethanol exposure. We focused on human glutamatergic neurons because of the well-documented effects of ethanol on glutamate signaling[18–21], the frontal cortex associations of GWAS findings[1], and SNP expression trait quantitative trait loci effects[22].

We used bulk RNAseq to characterize the effects of 7-day intermittent ethanol exposure (IEE) in glutamatergic neurons with endogenous GIRK2 levels. We then tested the combined effect of increased GIRK2 expression (↑GIRK2) and extended (7-21 days) IEE. We found downregulation of neuronal maturation and upregulation of metabolic and mitochondrial activity. To assess the functional consequences of this, we utilized multi-electrode arrays (MEA), calcium imaging, and patch-clamp electrophysiology in isogenic control (iso-CTL) and ↑GIRK2 neurons, collecting data on spontaneous as well as induced activity to study neuronal excitability. We followed up on the upregulated mitochondrial and metabolic genes, conducting mitochondrial stress tests in iso-CTL and ↑GIRK2 neurons with 7- and 21-day IEE, using glutamate stimulation to assess activity-dependent energy demands. Together, our results begin to elucidate the relationship between GIRK2, ethanol, glutamatergic signaling, and mitochondrial health.

METHODS

Astrocytes

Primary human fetal astrocytes (HFAs) were obtained from a commercial vendor and cultured in astrocyte medium according to the manufacturer specifications (ScienCell, Cat#: 1801). After cells have reached their terminal duplication capacity, they were transplanted onto 12mm glass acid-etched coverslips coated in 80ug/mL Matrigel (Thermo Fisher Scientific, Cat#: 08-774-552) and cultured for a week to achieve appropriate coverage and attachment.

Neural progenitor cells (NPCs) and induced neurons (iNs)

NPCs and dCas9-VPR NPCs from de-identified control hiPSC cell lines[17,26,64] were cultured in DMEM/F12 with sodium pyruvate GlutaMAX medium (Thermo Fisher Scientific, Cat#: 10565018) supplemented with FGF2 (Bio-Techne, Cat#: 233-FB), B27 (Life Technologies, Cat#: 17504-044), N2(Life Technologies, Cat#: 17502-048), and penicillin-streptomycin (Thermo Fisher Scientific, Cat#: 15-140-122). NPCs were induced

into neurons with doxycycline-inducible transcription factor *NGN2* with neomycin antibiotic selection (Addgene #99378), following the protocol described by [23]. Antibiotic selection was performed on Day 1 post-induction with 10 µg/mL neomycin sulfate (BioVision Incorporated, Cat#: 9620). Starting at Day 2 post-induction iNs were cultured in Neurobasal medium (Life Technologies, Cat#: 21103-049) supplemented with N2 and penicillin-streptomycin. At day 7 post-induction, iNs were infected with *KCNJ6* vector or *KCNJ6* gRNAs in dCas9-VPR expressing cell lines. At Day 10, iNs were dissociated using the Papain Dissociation System following the manufacturer's protocol (Worthington Biochemical Cat#: LK003153) and then transplanted onto HFA-covered coverslips with thiazovivin (1µg/mL) (EMD-Millipore, Cat#: 420220) to facilitate attachment. Starting at Day 14, B27 Plus culture system medium (Thermo Fisher Scientific, Cat#: A36534-01) supplemented with 2% fetal bovine serum (FBS) (Sigma Aldrich, Cat#: F3135) and 1% penicillin/streptomycin (Thermo Fisher Scientific, Cat#: 15-140-122) was introduced through half medium changes every other day to promote electrophysiological maturation.

KCNJ6 gRNA Design and Cloning

Single gRNAs were designed using CRISPR-ERA (http://crispr-era.stanford.edu/), with the predicted top six ranked guides selected for in-vitro validation. For lentiviral cloning, IDT synthesized oligonucleotides were annealed and phosphorylated using PNK (NEB#C3019) at 37° C for 30min, 95° C for 5min and ramp-down to 25° C at 5C/min. Annealed oligos were cloned into lentiGuide-TdTomato-Hygro (Addgene#99376) using BsmB1-v1 (NEB, discontinued) in an all-in-one T7 ligase (NEB#M0318S) based Golden-Gate assembly (37° C for 5min, 20°C for 5min x15 cycles), and subsequently transformed into NEB10beta (NEB#C3019). Purified DNA from propagated colonies were confirmed for gRNA insertion via Sanger sequencing (Genewiz). Following sanger confirmation, gRNAs were prepped for lenti-virus production.

Lentivirus preparation

Lentiviral vectors were prepared using PEI transfection of HEK-293T cells as previously described (Tiscornia et al., 2006). Viral titer was concentrated to 10^8 IU/mL. Vectors used are listed in Key Resources Table (Addgene #99378, #19780, #99347, #99376, #197032).

Intermittent Ethanol Exposure

Starting at Day 21 post-induction, pure ethanol (EtOH) (Sigma Aldrich, Cat# e7023) was added to B27 Plus System culture medium to achieve a concentration of 17 mM. A previous study demonstrated that after 24 h, ethanol concentration in medium is reduced to ~5 mM, therefore medium was "spiked" with 1ul EtOH/ 1.5 mL medium daily to maintain ~17 mM concentration [65].

Bulk RNAseq

NGN2-induced neurons were scraped from 12-well plates at 28 days of differentiation, spun down, and frozen. Total RNA extraction from frozen cell pellets, library preparation, and sequencing was performed by Genewiz (Azenta US, Inc., Indianapolis, IN). Total RNA was extracted from fresh frozen cell pellet samples using Qiagen RNeasy Plus Universal mini kit following manufacturer's instructions (Qiagen, Hilden, Germany). RNA samples were quantified using Qubit 2.0 Fluorometer (Life Technologies, Carlsbad, CA, USA) and RNA integrity was checked using Agilent TapeStation 4200 (Agilent Technologies, Palo Alto, CA, USA). RNA sequencing libraries were prepared using the NEB-Next Ultra RNA Library Prep Kit for Illumina using manufacturer's instructions (NEB, Ipswich, MA, USA). The samples were sequenced on the Illumina 4000 instrument, using a 2x150bp Paired End (PE) configuration. Image analysis and base calling were conducted by the Control software. Raw sequence data (.bcl files) generated the sequencer were converted into fastq files and de-multiplexed using Illumina's bcl2fastq 2.17 software.

Raw reads were assessed for quality using FastQC (version 0.11.8) before and after adapter sequence trimming by Cutadapt (version 4.1). Reads were pseudo-aligned using Salmon (version 0.13.1) for estimation of normalized gene expression (TPM, i.e. transcript per million). Reads were also aligned to the human reference genome (Gencode version 28) and quantified for gene read counts, both in STAR (version 2.5.3a). For differential gene expression analyses, read counts were modelled in the linear mixed model using batch, sex and donor information as the random effect terms and ethanol-treatment/control as the fixed effect term by the R (version 4.1.0) package "variancePartition" (version 1.28.0). The gene set enrichment analysis (GSEA) was performed with 1,000 permutations using R package GOtest (github.com/mw201608/GOtest) in the human molecular signatures database 'C2.CP','C5.BP','C5.CC' and 'C5.MF' collections.

Western blot

Tissue from 28-day-old neurons was collected by scraping and membrane protein was extracted using MemPer ThermoFisher kit (Thermo Fisher Scientific, Cat#: 89842) according to the manufacturer's instructions. The membrane fraction was then denatured for 20 minutes at 70°C in MES running buffer (Life Technologies, Cat#: B0002) and separated on a BOLT™ 4-12% Bis-Tris 1mm gel (Thermo Fisher Scientific, Invitrogen, Cat#: NW04125BOX) at 200mV for 20-30 minutes. Transfer to a nitrocellulose membrane was achieved using iBlot2. Membranes were then blocked in 5% milk in PBST for 1 hour. To ensure antibody specificity, antigen-competition was utilized as a control, where the antibody (Alomone, Cat #: APC-006) was pre-incubated with the antigen in the blocking solution for one hour on ice; 1:3 antibody to antigen ratio was used. Anti-NaK ATPase antibody (Cell Signaling Technology, Cat#: 23565S) was used as a loading control. Membranes were incubated in 1:500 antibody or antibody/antigen mixture overnight at 4°C. Anti-rabbit-HRP secondary antibody (Cell Signaling Technology, Cat#: 7074P2) at 1:1000 dilution was incubated for 1 hour at room temperature. Western-bright peroxidase (Advansta, Cat#: K-12045-D20) 2-minute incubation and 90s exposure on UVP imager were used to obtain images.

Immunocytochemistry

Neurons at day 28 were fixed in methanol for twenty minutes at -20°C, followed by permeabilization in 0.2% Triton-X in PBS (Mg^{2+}, Ca^{2+}), and blocking in 2% bovine serum albumin, 5% normal goat serum, 2% Triton-X in PBS (Mg^{2+}, Ca^{2+}) at room temperature. Primary antibodies were diluted in 4% NGS, 0.1% Triton in PBS (no Mg^{2+}, Ca^{2+}) (GIRK2 (Alomone, Cat #: APC-006) 1:400, TUJ1 (Biolegend, Cat#: 801213, RRID: AB_2728521) 1:1000) and incubated overnight at 4°C. Secondary antibodies were incubated for two hours at room temperature at 1:500 dilution [Anti-Rabbit AlexaFluor-488 (Thermo Fisher Scientific, Cat#: A-11008, RRID: AB_143165), Anti-Mouse AlexaFluor-647 (Thermo Fisher Scientific, Cat#: A-21235, RRID: AB_2535804)]. Images were acquired at the Icahn School of Medicine Microscopy and Advanced Biomaging Core, using the Zeiss Upright LSM-780, Axio Imager 2 confocal microscope with the 100x objective. Maximum intensity projection was obtained from Z-stacks consisting of 5-15 6.6 µm slices, using Zeiss Zen Black Software. The maximum intensity projection image was analyzed using the Analyze Particles option in FIJI (ImageJ)[66].

Multi Electrode Array (MEA)

CytoView 48-well MEA plates (Axion Biosystems, M768-tMEA-48B) were coated with 80ug/mL Matrigel (Thermo Fisher Scientific, Cat#: 08-774-552) and seeded with human fetal astrocytes (ScienCell, Cat#: 1801). Neurons were transplanted on Day 10 of induction. The plate was loaded onto the Axion Maestro MEA reader (Icahn School of Medicine at Mount Sinai Stem Cell Engineering Core), and the electrical activity was analyzed using AxIS 2.0 Neuronal Module Software. Recordings were acquired for 10 minutes at Days 28, 35, and 42 post-induction, approximately 24 h after last ethanol supplementation. Wells with < 0.01 Hz activity were excluded from analysis. One outlier data point was identified by the Grubbs outlier test and removed from further analysis.

Patch clamp electrophysiology

Day 42 neurons were recorded at room-temperature (~20^{o}C) in artificial cerebrospinal fluid (ACSF) external solution consisting of 125 mM NaCl, 5 mM KCl, 10 mM D-Glucose, 10 mM HEPES-Na, 3.1 mM $CaCl_2$, and 1.3 mM $MgCl_26{\cdot}H_2O$. Solution pH was adjusted to 7.4 with NaOH and filtered with 0.22 µM PEI bottle-top filter. Osmolarity was measured at 290-300 mOsm with VAPRO® Vapor Pressure Osmometer (Fisher Scientific, ELITechGroup Model 5600, Cat#: NC0044806). Patch pipettes were pulled to a resistance of 4-4.5 MΩ. GIRK current was recorded with an internal solution containing 140 mM K-D-Gluconate, 4 mM NaCl, 2 mM $MgCl_26{\cdot}H_2O$, 1.1 mM EGTA, 5 mM HEPES, 2 mM Na_2ATP, 5 mM Na-Creatine-PO_4, and 100 µM GTPγS. pH adjusted to 7.4, and osmolarity was measured at 300-310 mOsm. EPSCs were recorded gap-free at -70 mV using voltage-clamp with an internal solution of 135 mM CsCl2, mM 10 HEPES-Na, 1 mM EGTA, 1 Na mM–GTP, and 1 mM QX-314 as described by Yang et al., 2017[67].

Resting membrane potential was obtained in current-clamp mode (I = 0). Cells with a resting membrane potential higher than -40 mV and a membrane resistance lower than 100 MΩ were excluded from further recordings and analyses. For measuring excitability, the membrane potential was adjusted to -55 mV (equivalent to -72 mV with a junction-potential correction of 17 mV). Neuronal excitability was measured with current injection steps of 20 pA (up to 16 steps). Rheobase was defined as the voltage at which the first current injection step elicited an action potential first. Neurons with fewer than two action potential spikes were excluded from further analysis. In voltage-clamp, GIRK currents were assessed using a 100 ms voltage ramp (from -100 to 0 mV) to examine inward rectification of GIRK channels, followed by 300 ms pulse at -40 mV to measure the outward GIRK current, and a 20 ms step to -45 mV to monitor membrane

resistance, from a holding potential of -40 mV. Voltage pulses were delivered every 2 s at a sampling rate of 5.00 kHz, and lowpass filter frequency of 2 kHz. After 4-5 minutes 30 µM SCH-23390 (Fisher Scientific Cat#: 092550) in ACSF was applied for 1 minute, followed by a 2-minute ACSF washout. All data was acquired using the Clampex software (v11.0.3.3, Molecular Devices) with a Axopatch B200 amplifier and Digidata 1550B digitizer with HumSilencer enabled to minimize noise. EPSCs were analyzed with Easy Electrophysiology software (v2.5.2, Easy Electrophysiology). GIRK current quantification and I-clamp data were analyzed in Clampfit software (v10.7.0.3, Molecular Devices). The amplitude of GIRK currents were measured as an average of 20 ms at – 40 mV, approximately 150 ms after the voltage ramp.

Seahorse Assay

Assays were conducted at the Icahn School of Medicine Mitochondrial Analysis Facility, using an XFe96 Agilent Seahorse Analyzer. NPCs were plated directly in 96-well Agilent Seahorse Cell Culture plates (Agilent Technologies, Cat#: 101085-004), coated with Matrigel, and induced into neurons the following day. Each cell line was plated in 8-replicate wells for each experiment. On the day of the experiment, neurons were incubated for 1 hour in CO_2-free incubator in Agilent Seahorse DMEM assay medium (Agilent Technologies, cat# 103575-100) supplemented with 1 mM sodium pyruvate (Agilent Technologies, Cat#: 103578-100), 10 mM glucose (Agilent Technologies, Cat#: 103577-100), and 2 mM glutamine (Agilent Technologies, Cat#:103579-100). Acute 10 µM glutamate injection was applied to four replicate wells/donor/experiment during the mitochondrial stress test (Agilent Technologies, Cat#: 103015-100). The mitochondrial stress test was performed according to the manufacturer's protocol, with 1 µM oligomycin, 1 µM FCCP, 1 µM rotenone/antimycin-A. Data was acquired in Seahorse Wave software (Agilent Technologies).

After conclusion of the experiment, medium was aspirated and cells were fixed with Methylene blue overnight at 4° C. The dye was rinsed out the following morning with distilled water and cells were lysed with 4% acetic acid and 40% methanol. The lysate was transferred to a clear flat-bottom 96-well plate to measure absorbance at 595 nm using a Varioskan plate reader (Thermo Scientific, Cat#: VL0000D0) and SkanIt Software for Microplate Readers, ver. 6.0.2.3 (Thermo Scientific, Cat#: 5187139). Absorbance values were applied as a scaling factor for raw oxygen consumption rate (pmol/min) to normalize respiratory rate to cell density. Normalized raw data was exported as an Excel spreadsheet for further analysis in R Studio, v3.6.1 (R Core Team, 2020). Mitochondrial respiration parameters were calculated

according to the mitochondrial stress test assay user manual. Each experiment replicate is reported as the average of 4 wells.

Calcium Imaging

Neurons were incubated in 4 µM Fluo4-AM in ACSF (same solution as for patch clamp electrophysiology) for 20 minutes at 37° C, protected from light. Cells were then destained for an additional 5 minutes in ACSF at room temperature prior to imaging. Fluorescence was measured with at 10x objective on a Nikon TE2000 inverted microscope, 480 nm LED, excitation filter of (485 nm) and emission filter (530 nm). Images were obtained with a sCMOS Zyla 5.5 camera (Oxford Instruments, Andor), using a 10-fps rate and 4x4 binning under constant perfusion of ACSF in a laminar flow diamond-shaped chamber (Model #RC-25; Warner Instruments) at RT (~20° C). Spontaneous activity was recorded for 3 minutes. 10 µM glutamate in ACSF was applied in 30 second pulses, with a 1-minute ACSF washout period. 15 mM KCl in ACSF was applied at the end of the recording for 1 minute, followed by a 1-minute ACSF washout. Time of stimulus application was tagged during the recording.

Raw fluorescence data was collected using Nikon Elements software (NIS Elements AR; version 5.20.01). A background region of interest (ROI) was identified to subtract noise. ROIs were identified using automatic detection in Nikon Elements. All ROIs were manually curated and raw fluorescence data were exported into Excel. Subsequent analysis steps were carried out in R Studio (v3.6.1 of R). Each fluorescence trace was baseline-drift corrected using a penalized least-squares algorithm (AirPLS)[68] and $\Delta F/F_0$ was calculated according to the formula $(F_t-F_0)/F_0$, where F_0 was defined as the minimum fluorescence intensity (RFU) in the first 10s of the recording. Traces were filtered with a 3rd order Butterworth filter using "signal" package version 0.7-6[69] and spikes were detected using "Pracma" package version 2.3.3[70]. A neuronal spike was defined as <30s in duration and above 5 standard deviations of the background ROI. ROIs with astrocyte-like spikes (lasting > 30s) were excluded from the analyses.

Quantification and statistical analysis

All statistical analysis was carried out in R Studio, v3.6.1[71], using the following packages for quantitation and visualization: jtools version 2.1.4[72], lme4 version 1.1-27.1[73], ggplot2 version 3.3.5[74]. Generalized Linear Mixed Models (GLMM) were used for patch-clamp electrophysiology, MEA, calcium imaging, and

mitochondrial stress test data. Random effects included donor cell line and neuronal differentiation batch. Poisson distribution was specified for all spike count data. Student's t-test was used for immunocytochemistry puncta % μm^2 quantitation. All bar and line plots include +/- standard error of the mean.

RESULTS

Enhancing GIRK2 currents in human neurons using CRISPRa and lentiviral vector expression of KCNJ6

To study the effect of increased GIRK2 expression on neurogenin 2 (*NGN2*)-induced glutamatergic neurons[23] and their response to chronic ethanol exposure, we employed two different methodologies: dCas9-VPR activation (CRISPRa[17]) of the *KCNJ6* gene and expression from a lentiviral vector. CRISPRa has the advantage of upregulating the endogenously-encoded *KCNJ6* gene, but it relies on stable expression of the dCas9-coupled transcriptional activator VPR and chromatin accessibility of the endogenous gene[17,24]. Lentiviral vector-mediated expression bypasses these limitations, but expresses the *KCNJ6* mRNA without the 3'UTR, which may play a key role in protein trafficking to the plasma membrane as well as transcript stability[25].

We therefore evaluated the effect of both strategies on GIRK2 expression and function in *NGN2*-induced neurons using qPCR, Western blotting, and immunocytochemistry. The endogenous levels of GIRK2 protein appeared low, with average puncta density of 2.2 ± 0.5% of neuronal marker β-III tubulin (TUJ1)-immunoreactive area (μm^2). CRISPRa was accomplished using cell line 553 stably expressing dCas9-VPR[17] and co-expression of three pooled gRNAs targeting the KCNJ6 promoter (see Methods). In comparison to 553/dCas9-VPR alone, GIRK2 puncta density increased to 23 ± 3% ($p = 0.009$) in 553/dCas9-VPR + *KCNJ6* gRNAs (CRISPRa). For lentiviral (Lenti) expression of *KCNJ6*, we used a lentivirus containing the *KCNJ6* gene with mCherry red fluorescent marker in cell line 12455 (control line from Knight Alzheimer's Disease Research Center)[26]. Here, we observed an increase in GIRK2 puncta density to 24 ± 6% ($p = 0.005$) (N = 9-16 images/group) (**Figure 1A-B**). Thus, both CRISPRa- and Lenti-mediated *KCNJ6* expression appeared to increase the levels of GIRK2 protein expression similarly (**Figure 1A-B, Figure S1**).

We next examined whether higher protein expression led to an increase in GIRK current, using whole-cell patch-clamp electrophysiology. Both 553/dCas9-VPR and 12455/Lenti neurons were grown on glass coverslips for 5-6 weeks with human fetal astrocytes to improve maturation[27–29]. To study GIRK currents, we included 100 μM GTPγS in the internal solution to activate endogenous G proteins and produce

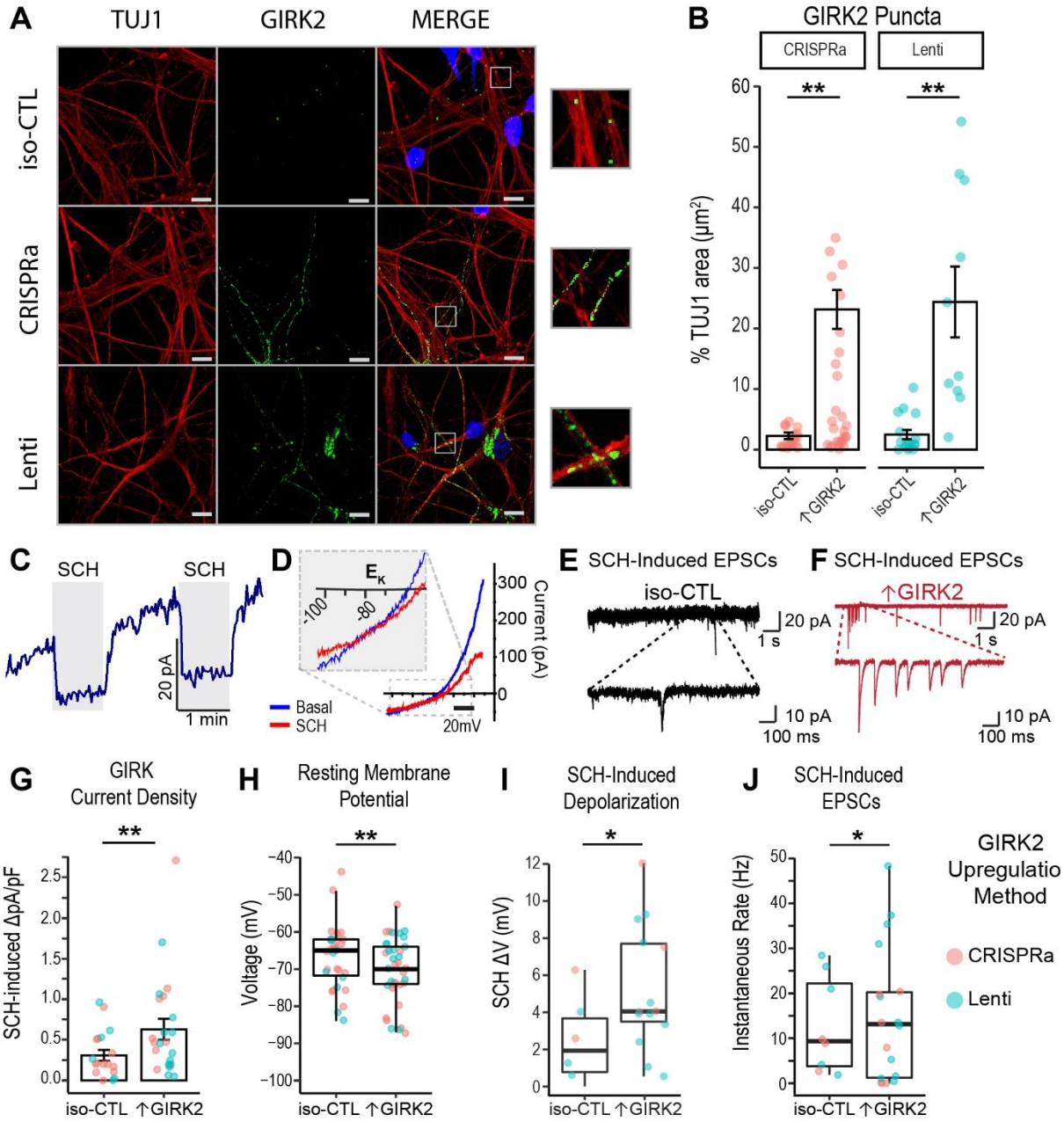

Figure 1. CRISPRa and lentiviral expression of GIRK2 both increase GIRK-current density and GIRK-mediated inhibition. A. Representative images of isogenic control (iso-CTL) neurons, CRISPRa- and Lenti-expression ↑GIRK2 neurons stained for TUJ1 (red), DAPI (blue), and GIRK2 (green); 100x magnification; scale bar and insets = 10 µm. **B.** Normalization of GIRK2 puncta µm^2 to TUJ1 µm^2; n = 2 donors; 3 coverslips; 3 images each. Each point represents a single image; coral = CRISPRa and teal = Lenti. **C.** Representative traces of GTPγS-activated current with two 1-min pulses of 30 µM SCH-23390 (grey rectangles) voltage-clamped at -40 mV. **D.** Representative current-voltage curves of basal (blue) and GIRK2-inhibited (SCH-23390l red) currents; inset: magnification of current reversal at the potassium equilibrium potential (E_K). **E-F:** Representative sEPSCs for iso-CTL (black) (**E**) and ↑GIRK2 (red) (**F**) neurons with SCH pulse. Main trace = 10 s, magnified inset = 1 s **G.** Bar graph of SCH-inhibited GIRK current density (mean ± SEM; pA/pF). **H.** Boxplot of resting membrane potential (n = 2 donors; 9-10 cells/group). Thick bar represents median, box represents first and third quartiles, and whiskers are 1.5*inter-quartile range. **I.** Boxplot shows change in resting membrane potential with SCH (n = 2 donors; 5-13 cells/group). **J.** Boxplot shows instantaneous sEPSC rate (Hz) with SCH (n = 2 donors; 8-17 cells/group). Statistics: generalized linear mixed model (GLMM) with donor and batch random effects. *p < 0.05, ** p < 0.01.

maximal GIRK activation, as previously described[30–32]. To confirm GIRK channel activation, we applied 30 µM SCH-23390 (referred to as SCH), which was shown previously to be a GIRK-specific-blocker[33,34]. At ~5 min following establishment of the whole-cell recording, SCH-application rapidly and reversibly inhibited the outward current (**Figure 1C**). The reversal potential for the SCH-inhibited current was approximately -80 mV (**Figure 1D**), which is near the calculated equilibrium potential for potassium (E_K) ($[K^+]_{out}$ = 5 mM, $[K^+]_{in}$ = 140 mM).

Overall, CRISPRa-mediated enhancement and lenti expression of *KCNJ6* led to similar increases in GIRK2 protein (**Figure 1A-B, Figure S1**); we therefore pooled these data and refer to them as ↑GIRK2. The GIRK current density for SCH-inhibited current was significantly larger in ↑GIRK2 neurons, as compared to isogenic controls (**Figure 1G**). Furthermore, ↑GIRK2 neurons exhibited more hyperpolarized resting membrane potentials (- 6.7 mV; N = 30-37 cells/group; p = 0.009) (**Figure 1H**), a larger SCH-induced membrane depolarization (+ 3.1 mV; N = 8-13 cells/group; p = 0.016) (**Figure 1I**), and a higher frequency of SCH-induced spontaneous EPSC (sEPSCs), (+ 7.9 Hz; N = 8-18 cells/group; p = 0.021) (**Figure 1E, F, & J**). ↑GIRK2 neurons did not significantly differ in rheobase, suggesting little impact of GIRK2 on action potential thresholds (see **Table S1**). Additional neuronal properties, including cell capacitance, membrane resistance, or evoked spiking activity revealed no significant differences (**Table S1**), indicating preservation of basic cell properties with ↑GIRK2. Collectively, these data support the conclusion of an increase in GIRK channel expression resulting in a functional increase in GIRK channel activity.

7-day 17 mM ethanol protocol: transcriptomic evidence of downregulated neuronal maturation and upregulated metabolic activity

Prior to investigating how ↑GIRK2 interacts with ethanol to influence neuronal activity, we first sought to investigate the effect of 17 mM ethanol (equivalent to 0.08% blood alcohol concentration) in iso-CTL neurons over 7 days on gene expression as determined by bulk RNAseq. We used an intermittent-ethanol-exposure (IEE) paradigm, described previously[6,35]. For IEE, we supplemented ethanol daily to maintain 17 mM concentration, since the ethanol concentration in the cell culture medium decreases to as low as 5 mM after 24h[6,35,36]. Glutamatergic neurons from four donors were induced in two batches in the absence of astrocytes to provide a pure neuronal population for RNAseq analyses. At day 21 post induction, when neurons begin to be electrically active[23], we treated half of the cultures with the IEE protocol for 7 days, and harvested the neurons at day 28 post-induction (**Figure 2A**).

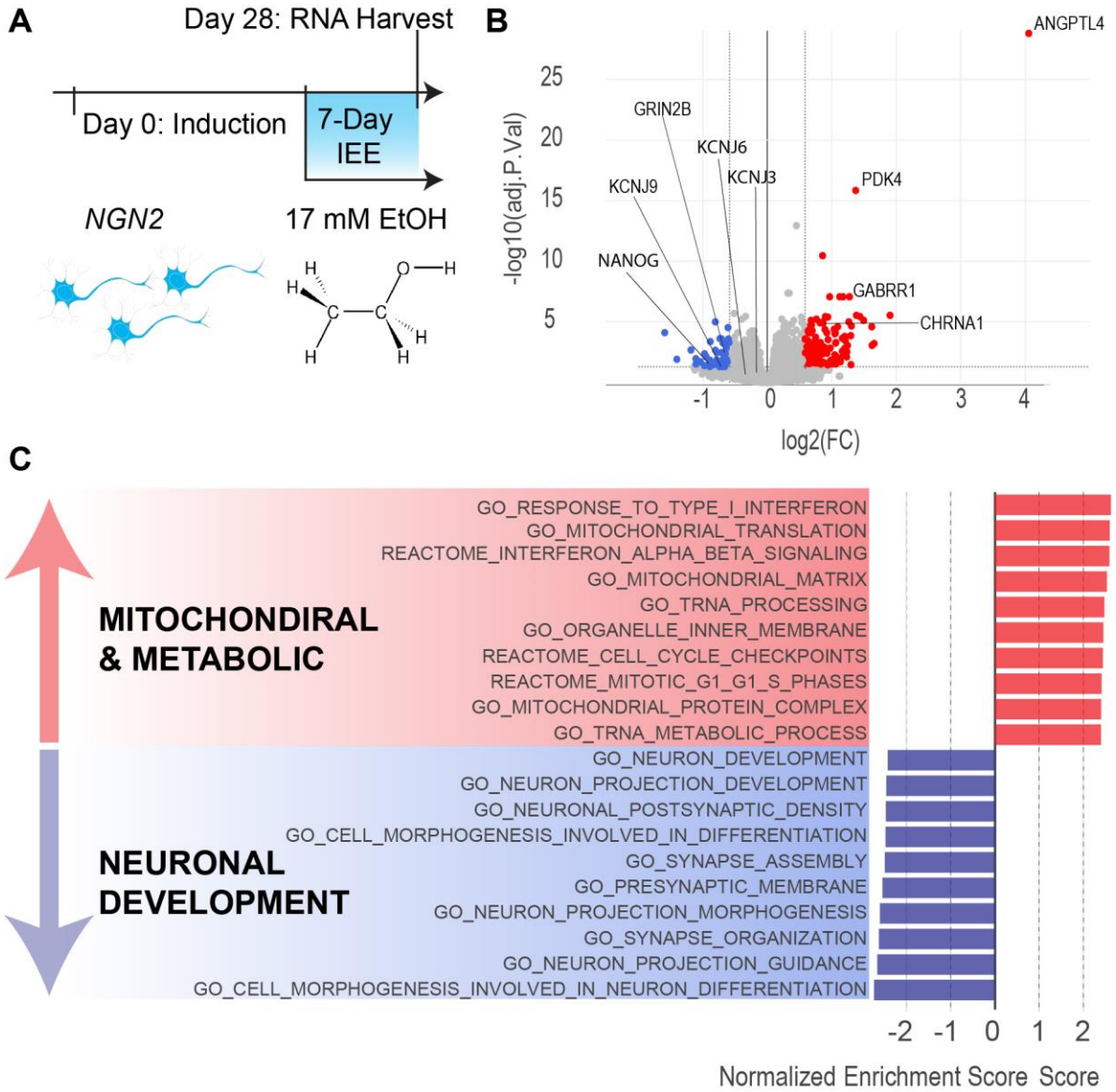

Figure 2. 7-Day Intermittent ethanol exposure (IEE) increases expression of mitochondrial and metabolic genes and impairs neuronal development genes. A. Timeline for neuronal induction, intermittent 17 mM ethanol exposure, and RNA harvest. **B.** Volcano plot of differentially expressed genes (fold-change = 1.5 and adjust p-value = 0.05 cutoffs). Blue dots represent downregulated genes and red dots represent upregulated genes. **C.** Gene ontology categories of differentially expressed genes. Bars depict normalized enrichment score (-log10(adjusted p-value) ≥ 5). N = 4 donors, 2 batches, 4 replicate wells.

Differential gene expression analysis revealed that 7-day IEE resulted in 127 upregulated and 50 downregulated genes, with Benjamini-Hochberg adjusted p-value cutoff of 0.05 and fold-change cutoff of 1.5 (**Figure 2B, Table S2**). Among them, *PDK4* and *ANGPTL4* showed the largest increase in fold-change. These two genes are involved in regulating the switch between glycolysis and fatty acid oxidation[37,38] and are both influenced by upstream proliferator-activated receptor-γ (PPARγ) [37,39]. Interestingly, *PDK4*

overexpression is associated with loss of metabolic flexibility and promotes excessive transport of calcium into mitochondria [38,40,41]. Gene ontology (GO) analysis shows the robust upregulation of the associated biological processes (**Figure 2D**). Most enriched categories are associated with metabolic, mitochondrial, and inflammatory pathways, suggesting one of the impacts of 7-day IEE is on energy utilization in glutamatergic neurons.

Furthermore, GO analysis revealed a significant downregulation of gene pathways involved in neuronal development, morphogenesis, and synapse organization - including transcription factor *NANOG*, voltage gated potassium channel subunit *KCNH1,* inwardly rectifying potassium channel subunit *KCNJ9*, and ionotropic glutamate receptor subunit *GRIN2B* (**Figure 2D, Table S2**). Expression of other inwardly rectifying potassium channels, including *KCNJ6* (GIRK2) and *KCNJ3* (GIRK1), and other canonical markers of glutamatergic identity, such as glutamate transporter *SCLA17A7* (vGLUT1) and glutamate receptor *GRIA4* (AMPAR), was not significantly affected (see **Table S3** for unabbreviated gene names). Interestingly, several genes involved in inhibitory neurotransmission were upregulated, including *CHRNA9* and *GABRR1* (**Figure 2C**)**.** Taken together, these data show that 7-day IEE promotes significant alterations in the transcriptome of glutamatergic neurons, indicating the presence of metabolic stress and diminished glutamatergic neuronal maturation.

GIRK2 expression counteracts hyperactivity induced by prolonged (7-21 days) 17 mM ethanol exposure

We hypothesized that ↑GIRK2 and IEE would act in concert to inhibit neuronal activity, because of ethanol-induced downregulation of neuronal maturation genes and the direct activation of GIRK channels[11]. To address this, we first used Multi-Electrode Arrays (MEA) to measure neuronal local field potentials over weeks of ethanol exposure. Using 553/dCas9-VPR and 12455/Lenti neurons, we started the IEE protocol at day 21, two weeks after the start of ↑GIRK2 expression (**Figure 3A**) and collected MEA data at days 28, 35, and 42, which were 1, 2 and 3 weeks, respectively, of ethanol exposure. MEA recordings were collected ~24 h after the last supplementation of ethanol, at a time when ethanol was ~5 mM in the culture medium[35] (**Figure 3B**).

At D28, MEA recordings showed very low levels of activity for both groups (**Figure 3C**). At days 35 and 42, however, IEE iso-CTL neurons exhibited a 1.49 Hz increase in weighted mean firing rate (WMFR) (**Figure 3D**, $p = 0.01$) and an 0.95 Hz increase in WMFR (**Figure 3E,** $p = 0.04$), respectively. By contrast, ↑GIRK2

neurons appeared unaffected by two weeks of IEE at day 35 (**Figure 3C**), but were significantly inhibited after three weeks of IEE at day 42, with a statistically significant interaction effect between increased GIRK2 expression and ethanol exposure (- 1.37 Hz WMFR; p = 0.02) (**Figure 3E**).

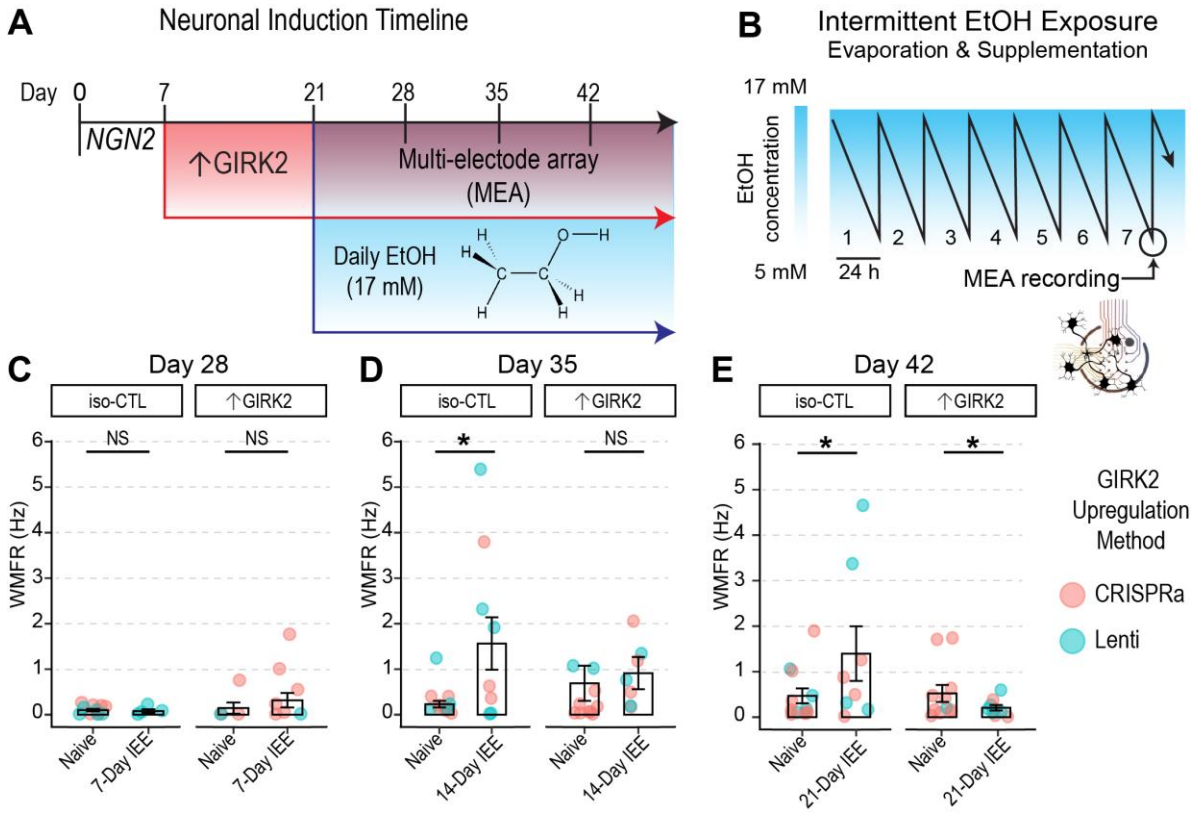

Figure 3. Increased GIRK2 expression counteracts hyperactivity induced by ethanol exposure in low-ethanol conditions. A. Timeline of neuronal differentiation, GIRK2 upregulation and ethanol exposure. **B.** Schematic of 7-day IEE, showing change in ethanol concentration over 24 hours due to evaporation[6,35]. **C-E**: Neuronal firing rates (WMFR) measured with multi-electrode array (MEA) is shown for *NGN2* neurons at Day 28 (1 week ethanol**) (C)**, 35 (2 weeks ethanol) **(D)**, and 42 (3 weeks ethanol) **(E)**; each point represents an MEA well; n = 2 donors| 5 batches. Point color indicates GIRK2 expression method (coral = CRISPRa; teal = Lenti). GLMM includes batch random effects. * p < 0.05.

GIRK2-upregulated neurons show inhibited spontaneous calcium spiking activity after 21-day IEE

To investigate the combined effects of 21-day IEE and ↑GIRK2 on glutamatergic neuronal activity under ethanol-free conditions, we conducted Ca^{2+} imaging, using Ca^{2+} transients as a proxy for neuronal activity. We expanded our donor pool to five cell lines (CRISPRa: 553/dCas9-VPR and 2607/dCas9-VPR; Lenti: 12455, 9429, and BJ) and carried out the same IEE protocol with *NGN2*-induced glutamatergic neurons, as described for the MEA experiments (**Figure 3A**). Ca^{2+} transients were detected with Fluo4-AM, and

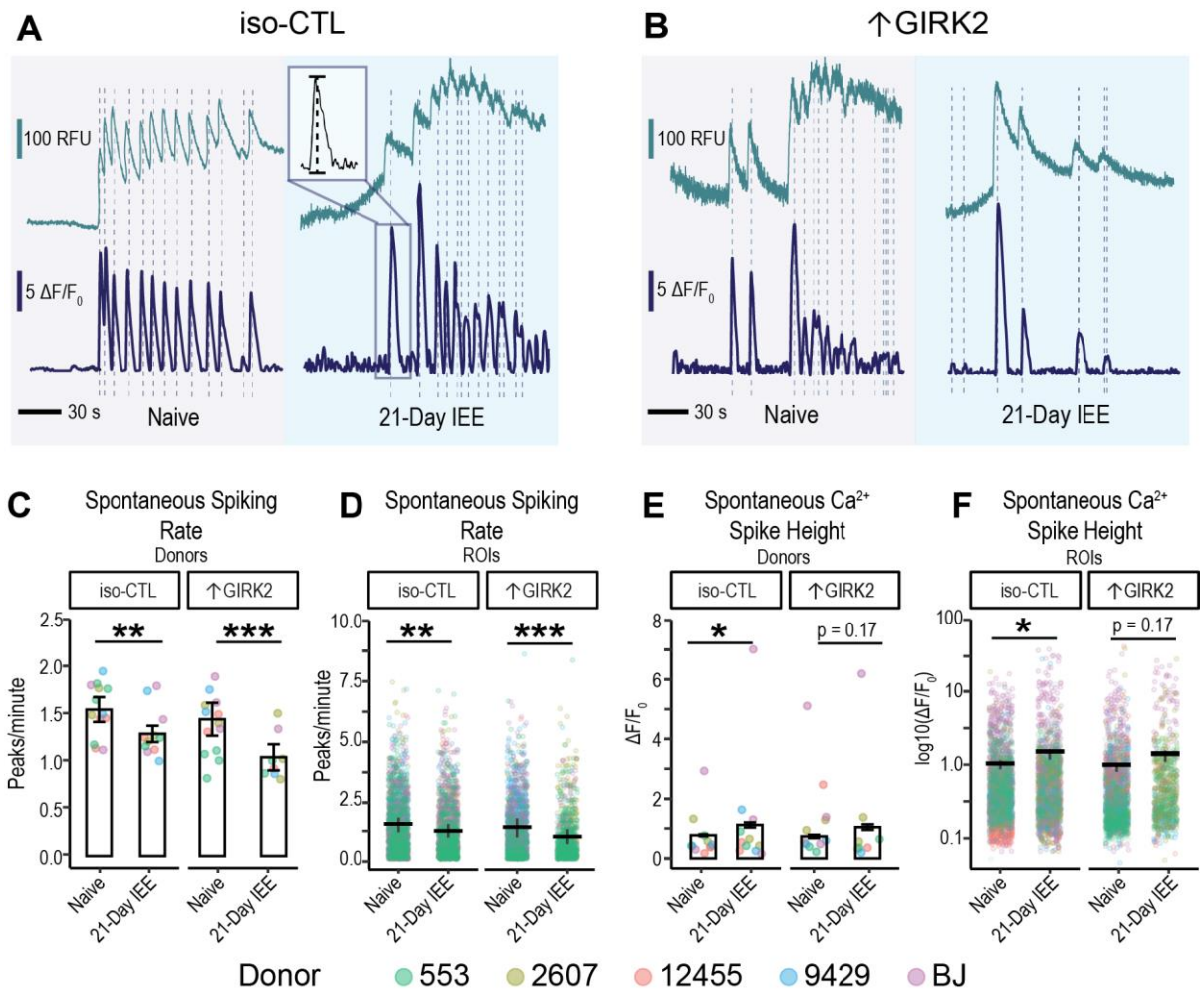

Figure 4. 21-Day IEE combines with ↑GIRK2 expression to inhibit spontaneous activity of excitatory neurons. A-B: Representative fluorescence traces showing Ca^{2+} spikes in alcohol-naïve (grey background) and 21-day IEE-treated (blue background) iso-CTL **(A)** and ↑GIRK2 **(B)** excitatory neurons on D42. Inset in iso-CTL: zoom of Ca^{2+} spike illustrating peak height measurement. Vertical dashed lines indicate auto detection of Ca^{2+} peaks. Top trace is raw fluorescence. Bottom trace is baseline-corrected $\Delta F/F_0$. Scale bars = 100 RFU, 5 $\Delta F/F_0$, and 30s. **C, D**: Ca^{2+} spike rate (peaks/minute) plotted as an average for each donor replicate (n = 5 donors, 3 replicates) **(C)** and as individual neuronal ROIs (n = 50 – 200 ROIs/replicate) **(D)**. **E- F:** Ca^{2+} transient height ($\Delta F/F_0$) plotted as an average for each donor replicate **(E)** and individual ROIs **(F)**. Color indicates donor (coral = 12455; dark yellow = 3440; green = 553; blue = 9429; and purple = BJ). GLMM includes replicate and donor random effects. * $p < 0.05$, ** $p < 0.01$, *** $p < 0.001$.

were baseline-corrected, filtered for non-neuronal events, and de-convolved to quantify peak frequency and height (**Figure 4A-B**) (N = 50-200 regions of interest (ROI)|5 donors|3 technical replicates).

Similar to MEA findings, IEE for 7 days significantly reduced the frequency of calcium spiking in spontaneously active neurons in ↑GIRK2 neurons in ethanol-free solution (-0.51 peaks/minute, $p < 0.00001$ IEE effect in ↑GIRK2 neurons; $p = 0.0006$ interaction IEE:↑GIRK2) (**Figure 4C-D**). One interpretation of this finding is that the inhibitory interaction of IEE with ↑GIRK2 is not caused by a direct

interaction of ethanol on GIRK2 channels. In contrast to MEA results, however, spontaneous Ca^{2+} activity decreased in IEE iso-CTL neurons measured under ethanol-free conditions, albeit to a lesser degree than ↑GIRK2 neurons (-0.19 peaks/minute, p = 0.003) (**Figure 4C-D**). IEE iso-CTL neurons also displayed a significant increase in calcium transient peak heights (+0.33 $\Delta F/F_0$, p =0.002) (**Figure 4E-F**), possibly indicating stronger depolarization. ↑GIRK2 neurons, on the other hand, showed no significant change in Ca^{2+} levels (+0.16 $\Delta F/F_0$, p = 0.10), suggesting that ↑GIRK2 expression ablates ethanol-induced increases in intracellular Ca^{2+}.

GIRK2 expression interacts with ethanol to differentially regulate glutamate sensitivity and intrinsic excitability

We hypothesized that, in addition to inhibiting spontaneous activity, 21-day ethanol exposure would alter neuronal excitability in ↑GIRK2 neurons. We interrogated neuronal excitability by bath-applying glutamate (10 µM for 30 s), which would be expected to depolarize neurons and elicit Ca^{2+} spikes. We measured the proportion of glutamate-responsive neurons, the number of Ca^{2+} peaks, the latency to the first spike, and the Ca^{2+} peak height. In iso-CTL neurons, 21-day IEE increased the proportion of glutamate-responsive neurons (+13.3%, p < 0 .001; N = 1203-2609 ROIs/group) (**Figure 5A**) as well as the number of glutamate-evoked spikes (+ 0.2 spikes, p = 0.02) (**Figure 5B, E**). These effects of IEE were absent in ↑GIRK2 neurons (**Figure 5A-B, F**). Furthermore, IEE decreased latency to first spike with glutamate in iso-CTL neurons, suggesting an increase in sensitivity to glutamate and/or excitability (-3.4 s, p < 0.00001) (**Figure 5C**). By contrast, 21-day IEE ↑GIRK2 neurons increased their latency to first spike with glutamate (+ 2.1 s, p = 0.0312 exposure effect; p < 0.00001 interaction effect) (**Figure 5C**). Similar to the measurements of spontaneous activity, (**Figure 4E-F**), calcium peak heights were significantly larger in IEE iso-CTL neurons (+ 0.36 $\Delta F/F_0$, p = $3x10^{-6}$), and this increase was not observed in ↑GIRK2 neurons (**Figure 5D**). Taken together, these data indicate that 21-day IEE heightens glutamate receptor activity and/or excitability in iso-CTL neurons, whereas ↑GIRK2 neurons exhibit diminished glutamate responses.

To determine whether differences in glutamate-responsive neurons were due to changes in glutamate sensitivity or in intrinsic excitability, we bath-applied 15 mM KCl in ACSF to directly depolarize the neurons (15 mM KCl is predicted to produce a ~32 mV positive shift in the resting membrane potential) and measured Ca^{2+} spikes in the same population of glutamate-responsive neurons. As before, Ca^{2+} flux was elevated in 21-day IEE iso-CTL neurons (+ 0.23 $\Delta F/F_0$, p < $1x10^{-6}$), while ↑GIRK2 neurons were unaffected

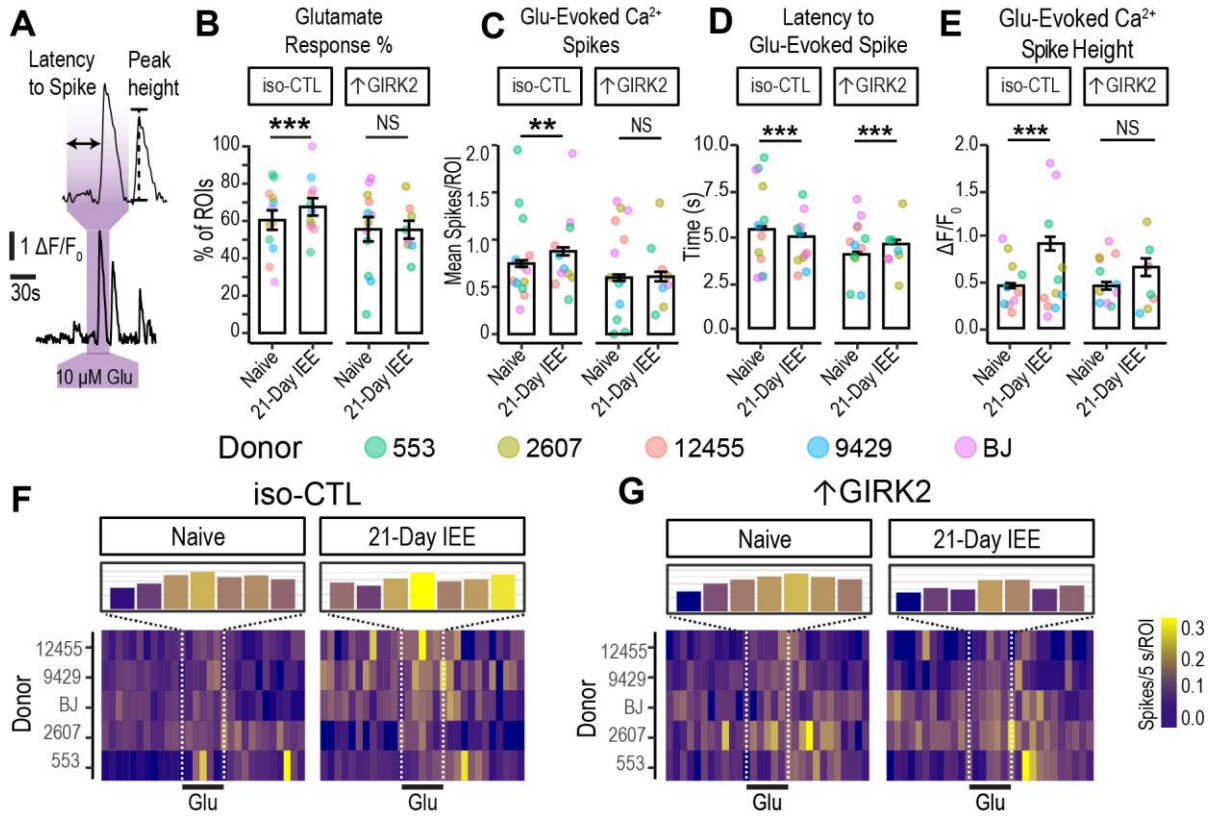

Figure 5. Increased GIRK2 expression combines with ethanol exposure to regulate glutamate sensitivity in excitatory neurons. A. Example deconvolved Ca^{2+} fluorescence trace, and latency to spike with a 30 s glutamate pulse. **B**. % of excitatory neurons responsive to 30 s glutamate pulse (10 μM), **C.** Number of calcium spikes during each 30s glutamate pulse, **D**. Latency to spike (s) in response to 30 s glutamate, pulse (10 μM). **E.** Calcium peak height ($\Delta F/F_0$) evoked by glutamate for iso-CTL and ↑GIRK2 neurons, either ethanol-naive or with 21-day IEE. Point color indicates donor (coral = 12455; dark yellow = 3440; green = 553; blue = 9429; and purple = BJ). **F, G.** Calcium spiking activity heatmap for iso-CTL **(F)** and ↑GIRK2 **(G)** neurons, either naive and with 21-day IEE. 5-second bins, normalized to number of cells (spikes/5 s/ROI). Inset magnification shows number calcium spikes/5 s/ROI during the 30 s pulse of 10 μM glutamate. Color gradient indicates activity intensity (violet = low; yellow = high). GLMM includes replicate and donor random effects. * $p < 0.05$, ** $p < 0.01$, *** $p < 0.001$

(**Figure 6D**). However, 21-day IEE in ↑GIRK2 neurons increased proportion of KCl-responsive ROIs (+8.3%, $p = 0.009$ IEE effect; $p < 1x10^{-6}$ interaction effect) (**Figure 6A**) and number KCl-evoked Ca^{2+} spikes (+ 0.54 spikes, $p < 1x10^{-6}$) (**Figure 6B**). Iso-CTL neurons, conversely, had a lower proportion of KCl-responsive ROIs (-16.5%, $p < 1X10^{6}$) (**Figure 6A**) and no difference in number of evoked spikes ($p = 0.4$) (**Figure 6B).** Iso-CTL neurons also increased their latency to spike in response to KCl (+ 6.7 s, $p = 0.0007$) (**Figure 6C**), and this change was also absent in ↑GIRK2 neurons ($p = 0.8$) (**Figure 6C**). These data indicate that, unlike glutamate-evoked activity, depolarization-evoked activity is suppressed in iso-CTL neurons and heightened in ↑GIRK2 neurons following 21-day IEE.

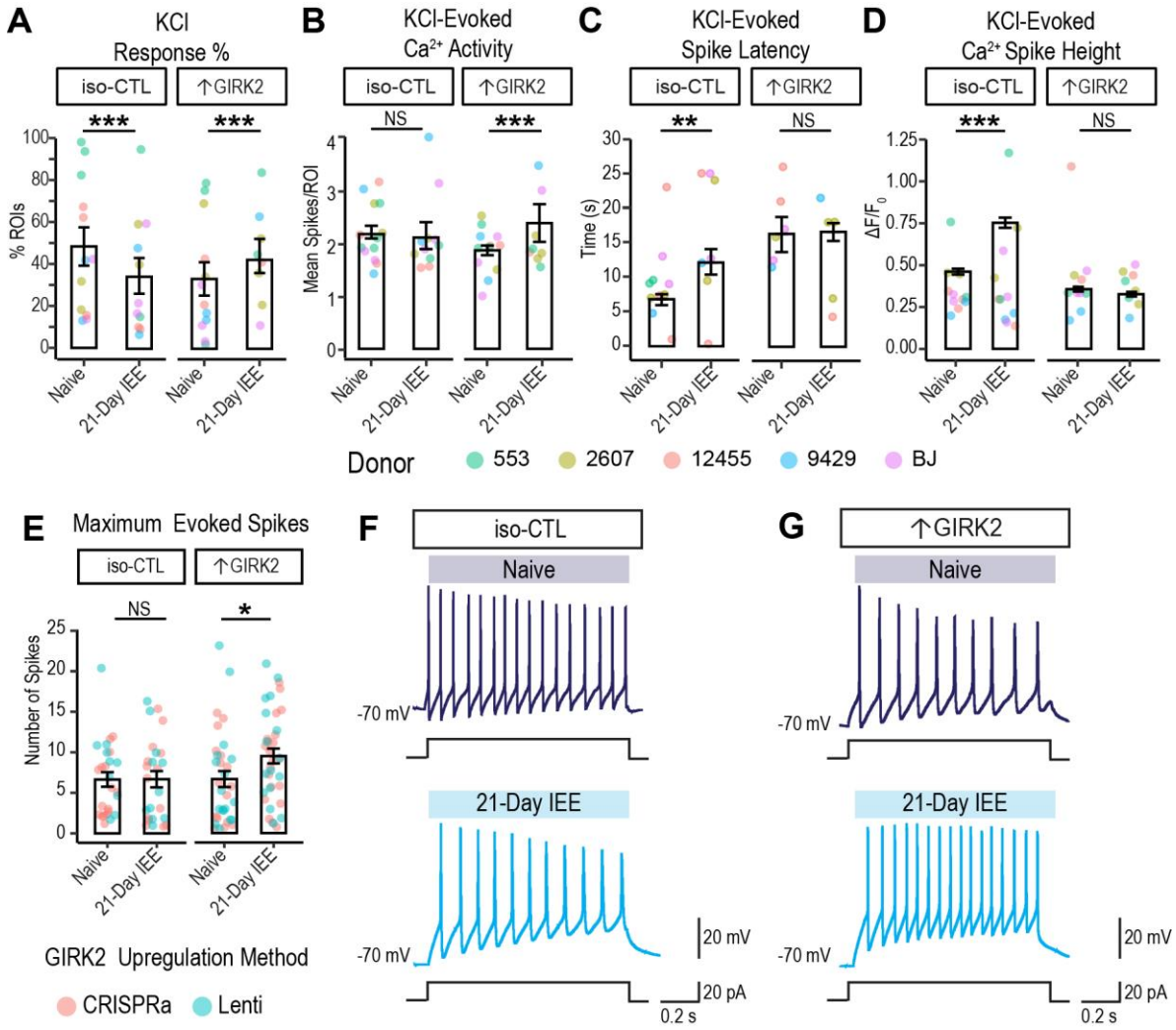

Figure 6. ↑GIRK2 neurons exhibit increased excitability after 21-Day IEE. A. % of ROIs responsive to 15 mM KCl (N = 1203-2608 ROIs/group). **B.** Number of spikes evoked by 1 min KCl pulse (15 mM). **C.** Latency to first spike (s) in response to 15 mM KCl pulse. **D.** Calcium spike height during 15 mM KCl pulse ($\Delta F/F_0$). **E.** Maximum number of evoked spikes measured in current-clamp with 20 pA current injection steps from holding potential of ~ -70 mV (N = 25-37 cells/group). **F**, **G:** Representative action potential traces evoked by a 1 s current injection (20 pA) step for CTL (**F**) and ↑GIRK2 (**G**) neurons, either for naive or 21-Day IEE neurons. GLMM includes batch and donor effects. * $p < 0.05$, ** $p < 0.01$, *** $p < 0.001$.

To further probe potential differences in intrinsic excitability, we examined the maximum number of spikes induced with depolarizing current injection steps (20 pA) using whole-cell patch-clamp electrophysiology (**Figure 6E-G**). Similar to KCl-induced firing (**Figure 6B**), there was no significant difference in the number of spikes for iso-CTL neurons with 21-day IEE. By contrast, we recorded a higher number of spikes in ↑GIRK2 neurons with 21-day IEE (+2.8 spikes, $p = 0.002$) (**Figure 6E-G**), similar to that

with KCl-induced firing. Taken together, these results suggest inhibitory effects of ↑GIRK2 with 21-day IEE appear to be specific to glutamate-mediated activity.

Impact of ethanol exposure, GIRK2 expression, and glutamate on mitochondrial function in excitatory neurons

Mitochondria serve as regulators of intracellular calcium, and this function has been shown to be disrupted with chronic alcohol use[42–45]. In support of ethanol-disrupted mitochondrial function, our bulk RNAseq results indicate upregulation of metabolic and mitochondrial genes after 7-day IEE (**Figure 2D**). Moreover, the changes in intracellular neuronal Ca^{2+}, as inferred from Ca^{2+} peak heights, during basal (**Figure 4E-F**), glutamate-evoked (**Figure 5D**), and KCl depolarization-evoked (**Figure 6D**) activity in 21-day IEE iso-CTL neurons, could also reflect changes in mitochondrial performance. We therefore investigated the effect of IEE and ↑GIRK2 on mitochondrial function. We hypothesized that ↑GIRK2 would prevent changes in cellular respiration caused by 7-day and 21-day IEE, similar to the inhibitory effect on increased calcium activity.

To test this prediction, we utilized the mitochondrial stress test (Agilent Technologies Seahorse assay) with monocultures of glutamatergic neurons (monocultures eliminate the potential confound of glial cells). Respiration was measured in ethanol-free conditions at day 28 post-induction with 7-day IEE and at day 42 with 21-day IEE (N = 5 donors|4 wells|3 batches/timepoint) and normalized for cell density. Seven-day IEE resulted in significant impairment of basal (-17.5 pmol/min/cell oxygen consumption rate (OCR), p = 0.03) (**Figure 7A** and **7C**) and maximal (-72.6 pmol/min/cell OCR, p = 0.04) (**Figure 7A** and **7D**) cellular respiration in iso-CTL neurons. By contrast, ↑GIRK2 neurons appeared less sensitive to IEE (- 10.5 pmol/min/cell OCR, p = 0.61). This decrease in respiration in IEE iso-CTL neurons may be the stimulus for upregulation of mitochondrial and metabolic genes as measured in RNAseq (**Figure 2D**), serving as a potential compensatory mechanism.

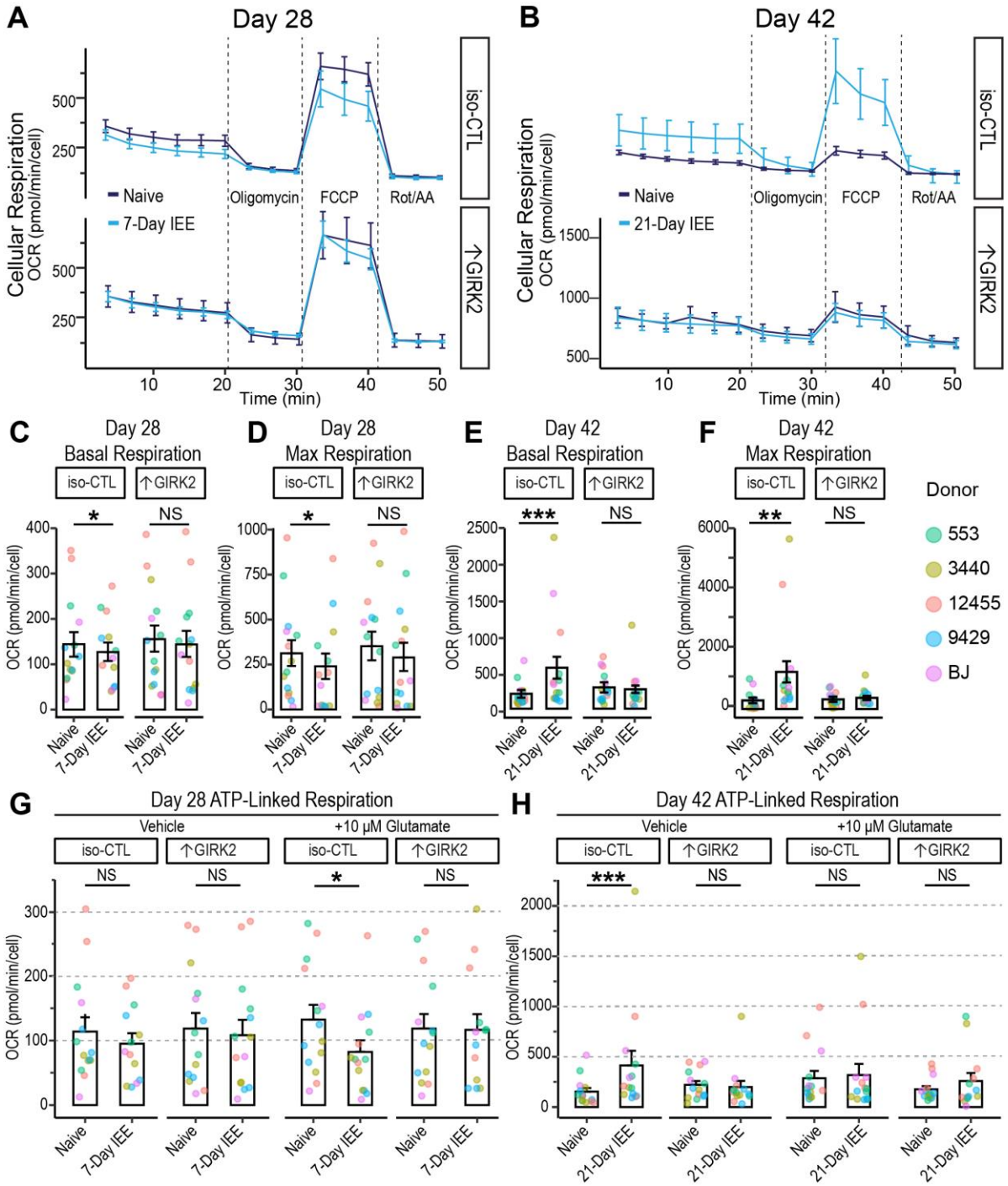

Figure 7. ↑GIRK2 expression counteracts metabolic adaptations to IEE. A-B: Time course of cell-density-normalized oxygen consumption rate (OCR; pmol/minute/cell) during the mitochondrial stress test in CTL and ↑GIRK2 neurons at Day 28 (7-day IEE) **(A)** and Day 42 (21-day IEE) **(B)** post-induction. Line color indicates ethanol exposure: dark blue = naive, light blue = IEE. **C-F:** Day 28 post-induction basal **(C)** and maximal OCR (pmol/min/cell) **(D)** and D42 basal **(E)** and maximal **(F)** OCR in WT and ↑GIRK2 neurons naive to ethanol or with IEE. **G-H:** ATP linked respiration in D28 **(G)** and D42 **(H)** neuron naive to ethanol or with IEE during basal (vehicle) and stimulated (10 μM glutamate) conditions (pmol/min/cell). Each point represents and average of 4 wells from 3 replicate experiments (N = 5 donors). Point color indicates donor (coral = 12455; dark yellow = 3440; green = 553; blue = 9429; purple = BJ). GLMM includes donor and batch effects. * $p < 0.05$, ** $p < 0.01$, *** $p < 0.001$.

At day 42, the overall oxygen consumption rate was higher than at day 28 (**Figure 7A-F**), reflecting a parallel between increased neuronal activity (**Figure 3C-E**) and increased oxygen consumption. Twenty-one-day IEE significantly increased oxygen consumption during basal (352 pmol/min/cell OCR, p = 0.0006) (**Figure 7E**) and maximal (928 pmol/min/cell OCR, p = 0.00003) (**Figure 7F**) respiration in iso-CTL neurons. Notably, ↑GIRK2 neurons did not show the increase in basal or maximal respiration with 21-day IEE (**Figure 7B**). Statistical analysis indicates an interaction between ↑GIRK2 and ethanol exposure for both basal (p = 0.02) (**Figure 7E**) and maximal (p = 0.009) (**Figure 7F**) respiration. These results suggest a degree of resilience and potential pro-allostatic influence from ↑GIRK2.

To test whether these changes were reflective of activity-dependent energy demands, we stimulated neuronal activity with an acute injection of 10 µM glutamate and measured ATP-linked respiration (**Figure S2 A**). At day 28, we observed no differences in ATP-linked respiration at basal levels of activity, regardless of ethanol exposure or GIRK2 expression levels (**Figure 7G**). The glutamate (10 µM) challenge, on the other hand, reduced ATP-linked respiration in IEE iso-CTL (- 66.3 pmol/min/cell OCR, p = 0.017) but not in ↑GIRK2 neurons (p = 0.49) (**Figure 7G**). This suggests an initial impairment in the ability of iso-CTL neurons to meet activity-dependent energy demands, which are likely lessened by ↑GIRK2 expression.

At day 42, iso-CTL neurons exhibited a surge in ATP-linked respiration (+260 pmol/min/cell OCR, p = 0.03) (**Figure 7H**) under basal conditions, consistent with the observed increases in basal (**Figure 7E**) and maximal (**Figure 7F**) oxygen consumption rate. Interestingly, the glutamate (10 µM) challenge eliminated these effects, boosting respiration in ethanol-naïve neurons and dampening respiration in ethanol-exposed iso-CTL neurons. Since ethanol exposure increases glutamate sensitivity and firing in iso-CTL neurons, these findings support the conclusion of increased energy demands and the involvement of compensatory mechanisms. In line with the reduced glutamate response evident in Ca^{2+} imaging (**Figure 5A-E**), ATP-linked respiration remained unchanged in ↑GIRK2 neurons following 21-day IEE (p = 0.57) (**Figure 7H**).

Overall, these data represent a progression from an initial impairment to a subsequent surge of mitochondrial function as a result of prolonged ethanol exposure. Our findings also suggest that ethanol exposure confers a metabolic challenge, which is exacerbated by the presence of elevated glutamate. Increased GIRK2 expression appears to prevent this trajectory, as evidenced by unaltered cellular respiration regardless of ethanol exposure or glutamate challenge.

DISCUSSION

In the current study, we employed an isogenic approach to directly examine the functional effects of GIRK2 channels in human excitatory glutamatergic neurons, and to determine their response to physiological concentrations of ethanol over 21 days. We hypothesized that increases in GIRK2 expression would impact neuronal adaptations to ethanol exposure, either through its direct interaction via an alcohol-binding pocket in GIRK2, and/or through secondary mechanisms and regulation of neuronal excitability. We found that increased GIRK2 expression (↑GIRK2) mitigates changes in neuronal activity and mitochondrial respiration induced by 21-day intermittent 17 mM ethanol exposure.

↑GIRK2 neurons exhibited more hyperpolarized resting potentials, and larger GIRK-like currents (SCH-inhibited), as expected for an inwardly-rectifying potassium channel[8,33,34]. Interestingly, some of the changes in spontaneous neuronal activity induced with IEE (i.e., increased local field potential firing and increased Ca^{2+} transient size) were absent in ↑GIRK2 neurons. We explored whether these changes occurred through differences in glutamate receptor activation or intrinsic excitability. Several findings indicated a change in excitability with ↑GIRK2 expression and suppression of IEE-induced increase in glutamate sensitivity. The increase in neuronal activity with glutamate (i.e., increased % of responsive ROIs, decreased latency to spike, and increased number of spikes/30 s pulse) following IEE was blunted by ↑GIRK2. Unexpectedly, direct depolarization with 15 mM KCl during calcium imaging as well as with current injection steps during patch-clamp electrophysiology had an opposite effect — ↑GIRK2 neurons appeared to be more excitable following IEE. This may be attributable to a reduction in voltage-dependent inactivation of Na^+ and K^+ channels, possibly as a consequence of hyperpolarization in ↑GIRK2 neurons with IEE.

Together, these findings point towards a specificity of the anti-excitatory synergistic effect of IEE and ↑GIRK2 expression on glutamate-receptor-dependent signaling. The selective influence of GIRK2 on glutamate sensitivity may be linked to Group II metabotropic glutamate receptor signaling[46,47]. Group II mGluRs are $G_{i/o}$ GPCRs and act as presynaptic autoreceptors, facilitating feedback inhibition of glutamate release[48]. Several studies have shown Group II mGluR agonism inhibits network excitability[48,49] and have investigated their potential as a therapeutic interventions in AUD [50].

Increased GIRK2 expression in neurons may also help maintain normal mitochondrial function. Recent work by Sun *et al.* showed that glutamatergic neurons metabolize ethanol, using it as a preferred energy source over glucose in chronic ethanol exposure conditions[51]. Mitochondria are vulnerable to ethanol-

induced metabolic changes[52–54] and their regulation of calcium homeostasis plays a key role in excitotoxicity[42,44,45]. This appears to be consistent with the possibly compensatory upregulation of mitochondrial and metabolic genes after 7-day IEE. Notably, investigations in iPSC-neurons demonstrated the overall impact of ethanol exposure on mitochondrial health and neuronal development [55,56], including upregulation of genes involved in cholesterol homeostasis (*INSIG1* and *LDLR*)[57]. Despite a much lower concentration of ethanol in our paradigm (17mM vs. 50mM in Jensen *et al.,* 2019[57]), our results are similar: the top two upregulated genes in our 7-day ethanol exposure paradigm (*ANGPTL4* and *PDK4*) (**Figure 3B**) are also key players in lipid metabolism; *PDK4* in particular, has been associated with a loss of metabolic flexibility[40,41] and disrupted mitochondrial homeostasis[38]. Interestingly, GIRK channel activity is potentiated by cholesterol[12,58], suggesting that changes in membrane cholesterol could impact GIRK function.

We discovered that adaptations in mitochondrial respiration to both 7-day and 21-day IEE were altered in ↑GIRK2 neurons, which appeared to maintain normal mitochondrial function, regardless of ethanol exposure (7- and 21-day IEE) or activity-dependent energy demand. By contrast, stimulation of neuronal activity in iso-CTL neurons with glutamate revealed an impairment in ATP-linked respiration after 7-day IEE, indicating a difficulty in meeting activity-dependent energy demands. Furthermore, after 21-day IEE, glutamate eliminated the increase of ATP-linked respiration in iso-CTL neurons. The reduction of ATP-linked respiration with the application of glutamate may be attributable to increased calcium influx and the disruption of mitochondrial membrane potential[42,44].

↑GIRK2 expression also prevented increases in calcium peak heights induced by IEE in iso-CTL neurons. Since elevated intracellular calcium is a hallmark of excitotoxicity[42], GIRK2-mediated inhibition in ethanol-exposed glutamatergic neurons may serve a protective role. GIRK channels are essential mediators of synaptic depotentiation[59]. Calcium influx through NMDAR channels has been shown to increase surface expression of GIRK channels[59], supporting the conclusion that GIRK channel expression is linked to fluctuations in glutamatergic signaling.

In support of our finding that the upregulation of GIRK2 plays an important role in controlling neuronal excitability as well as modulating the response to ethanol, a recent study found that iPSC-derived human neurons derived from AUD-diagnosed participants containing specific *KNJ6* SNPs had lower levels of GIRK2 expression, greater neurite area, and heightened excitability than neurons derived from unaffected individuals[6]. Overexpression of GIRK2 in neurons from AUD-diagnosed individuals mimicked the effects of

the 7-day IEE protocol, eliminating differences in neuronal morphology induced excitability[6]. Thus, in the context of AUD, increased GIRK2 expression and subsequent neuronal inhibition appears to exert a normalizing influence.

On the other hand, previous studies investigating the role of GIRK2 expression in neuronal health showed somewhat conflicting outcomes. One demonstrated that GIRK2 expression in TH-positive substantia nigra dopaminergic neurons is a vulnerability factor to mitochondrial stress and apoptosis[60]. Another found that GIRK2 is upregulated in response to neurotoxins such as $A\beta_{42}$ in hippocampal dissociated cultures, potentially triggering $p75^{NTR}$ mediated cell-death[61]. Notably, $A\beta_{42}$ has an excitotoxic effect, similar to the consequences of long-term ethanol exposure[62], and therefore GIRK2 upregulation could be a protective measure.

Given the broad expression of GIRK channels as well as the regional and cell-type variability of their impact on neuronal activity, our observation could be unique to maturing glutamatergic neurons in the absence of inhibitory control. A dissection of the relationship between GIRK2 activity and cellular respiration is necessary to fully elucidate the channel's role in neuronal health and resilience. Several key questions remain, including whether basal GIRK channel activity is essential for preserving mitochondrial function and whether increasing GIRK2 expression after the start of ethanol exposure would have a similar ameliorating effect. Future investigations are necessary to determine the mechanisms underlying the intersection of GIRK channels, metabolism, and electrophysiology, and whether initial levels of GIRK channel expression can serve as an indicator for pharmacotherapy selection. In summary, we demonstrate that GIRK2 expression impacts the long-term effects of ethanol on spiking activity and bioenergetics of glutamate neurons. This suggests a possible role for GIRK2 in mitigating hyper-glutamatergic adaptations and mitochondrial dysfunction caused by chronic alcohol use.

Limitations of the study

Our study was not designed to discern the influence of non-coding regions on GIRK2 channel expression and function, in part limited by the low number of dCas9-VPR expressing cell lines (N = 2). Future studies should expand this donor pool to elucidate the impact of specific non-coding variation in *KCNJ6,* incorporating techniques to assess RNA stability and protein trafficking. Another limitation is our use of pure glutamatergic neuronal cultures. Further investigation is required to dissect the contribution of other

neuronal types, including co-culture with- or monocultures of GABA and dopamine neurons. Astroglia also warrant inclusion as a variable in assessing glutamate sensitivity and metabolism. Although GIRK expression is limited to neurons[63], its presence can nonetheless impact the balance of the tripartite synapse. Furthermore, functional differences between GIRK2 homotetramer and GIRK1/2 heterotetramer channels may affect adaptations in neuronal excitability. Together, these investigations can answer the question of cell-type specificity of the effects of GIRK2 on neuronal health and its interactions with ethanol.

ACKNOWLEDGMENTS

We gratefully acknowledge the support provided by the Ruth L. Kirschstein National Research Service Award (NRSA) Individual Predoctoral Fellowship (1 F31AA027949-01), and Collaborative Studies on the Genetics of Alcoholism (National Institute on Alcohol Abuse and Alcoholism; NIAAA U10AA008401). Special thanks to Dr. Kristen Brennand and Dr. Julia TCW for providing NPC cell lines used in this study. Additional thanks to Dr. Edoardo Marcora for consultation on generalized linear mixed model statistical analysis.

The Collaborative Study on the Genetics of Alcoholism (COGA), Principal Investigators B. Porjesz, V. Hesselbrock, T. Foroud; Scientific Director, A. Agrawal; Translational Director, D. Dick, includes eleven different centers: University of Connecticut (V. Hesselbrock); Indiana University (H.J. Edenberg, T. Foroud, Y. Liu, M. Plawecki); University of Iowa Carver College of Medicine (S. Kuperman, J. Kramer); SUNY Downstate Health Sciences University (B. Porjesz, J. Meyers, C. Kamarajan, A. Pandey); Washington University in St. Louis (L. Bierut, J. Rice, K. Bucholz, A. Agrawal); University of California at San Diego (M. Schuckit); Rutgers University (J. Tischfield, R. Hart, J. Salvatore); The Children's Hospital of Philadelphia, University of Pennsylvania (L. Almasy); Virginia Commonwealth University (D. Dick); Icahn School of Medicine at Mount Sinai (A. Goate, P. Slesinger); and Howard University (D. Scott). Other COGA collaborators include: L. Bauer (University of Connecticut); J. Nurnberger Jr., L. Wetherill, X., Xuei, D. Lai, S. O'Connor, (Indiana University); G. Chan (University of Iowa; University of Connecticut); D.B. Chorlian, J. Zhang, P. Barr, S. Kinreich, G. Pandey (SUNY Downstate); N. Mullins (Icahn School of Medicine at Mount Sinai); A. Anokhin, S. Hartz, E. Johnson, V. McCutcheon, S. Saccone (Washington University); J. Moore, Z. Pang, S. Kuo (Rutgers University); A. Merikangas (The Children's Hospital of Philadelphia and University of Pennsylvania); F. Aliev (Virginia Commonwealth University); H. Chin and A. Parsian are the NIAAA Staff Collaborators. We continue to be inspired by our memories of Henri Begleiter and Theodore Reich,

founding PI and Co-PI of COGA, and also owe a debt of gratitude to other past organizers of COGA, including Ting- Kai Li, P. Michael Conneally, Raymond Crowe, and Wendy Reich, for their critical contributions. This national collaborative study is supported by NIH Grant U10AA008401 from the National Institute on Alcohol Abuse and Alcoholism (NIAAA) and the National Institute on Drug Abuse (NIDA).

AUTHOR CONTRIBUTIONS

IP, AG, PAS conceived the project. IP and MBF performed experiments. IP and YL performed statistical analyses and discussed with PAS and AG. AG, PAS, RPH, ZPP, IGR, DP provided critical feedback throughout the project. IP, PAS prepared the paper with critical evaluation from RPH, ZPP, JST, BP, HJE, XX, DPC, CM. CM, RPH, HJE, and BP edited the manuscript.

DECLARATION OF INTERESTS

The authors declare no competing interests.

REFERENCES

1. Kang, S.J., Rangaswamy, M., Manz, N., Wang, J.-C., Wetherill, L., Hinrichs, T., Almasy, L., Brooks, A., Chorlian, D.B., Dick, D., et al. (2012). Family-based Genome-wide Association Study of Frontal Theta Oscillations Identifies Potassium Channel Gene KCNJ6. Genes Brain Behav. *11*, 712–719. 10.1111/j.1601-183X.2012.00803.x.

2. Kamarajan, C., Pandey, A.K., Chorlian, D.B., Manz, N., Stimus, A.T., Edenberg, H.J., Wetherill, L., Schuckit, M., Wang, J.-C., Kuperman, S., et al. (2017). A KCNJ6 gene polymorphism modulates theta oscillations during reward processing. Int. J. Psychophysiol. Off. J. Int. Organ. Psychophysiol. *115*, 13–23. 10.1016/j.ijpsycho.2016.12.007.

3. Chorlian, D.B., Rangaswamy, M., Manz, N., Meyers, J.L., Kang, S.J., Kamarajan, C., Pandey, A.K., Wang, J.-C., Wetherill, L., Edenberg, H., et al. (2017). Genetic correlates of the development of Theta Event Related Oscillations in Adolescents and Young Adults. Int. J. Psychophysiol. Off. J. Int. Organ. Psychophysiol. *115*, 24–39. 10.1016/j.ijpsycho.2016.11.007.

4. Jones, K.A., Porjesz, B., Chorlian, D., Rangaswamy, M., Kamarajan, C., Padmanabhapillai, A., Stimus, A., and Begleiter, H. (2006). S-transform time-frequency analysis of P300 reveals deficits in individuals diagnosed with alcoholism. Clin. Neurophysiol. Off. J. Int. Fed. Clin. Neurophysiol. *117*, 2128–2143. 10.1016/j.clinph.2006.02.028.

5. Rangaswamy, M., Jones, K.A., Porjesz, B., Chorlian, D.B., Padmanabhapillai, A., Kamarajan, C., Kuperman, S., Rohrbaugh, J., O'Connor, S.J., Bauer, L.O., et al. (2007). Delta and Theta oscillations as risk markers in Adolescent Offspring of Alcoholics. Int. J. Psychophysiol. Off. J. Int. Organ. Psychophysiol. *63*, 3–15. 10.1016/j.ijpsycho.2006.10.00.

6. Popova, D., Gameiro-Ros, I., Youssef, M.M., Zalamea, P., Morris, A.D., Prytkova, I., Jadali, A., Kwan, K.Y., Kamarajan, C., Salvatore, J.E., et al. (2023). Alcohol reverses the effects of KCNJ6 (GIRK2) noncoding variants on excitability of human glutamatergic neurons. Mol. Psychiatry *28*, 746–758. 10.1038/s41380-022-01818-x.

7. Mayfield, J., Blednov, Y.A., and Harris, R.A. (2015). Behavioral and Genetic Evidence for GIRK Channels in the CNS: Role in Physiology, Pathophysiology, and Drug Addiction. Int. Rev. Neurobiol. *123*, 279–313. 10.1016/bs.irn.2015.05.016.

8. Lüscher, C., and Slesinger, P.A. (2010). Emerging concepts for G protein-gated inwardly rectifying potassium (GIRK) channels in health and disease. Nat. Rev. Neurosci. *11*, 301–315. 10.1038/nrn2834.

9. Glaaser, I.W., and Slesinger, P.A. (2015). Structural Insights into GIRK Channel Function. Int. Rev. Neurobiol. *123*, 117–160. 10.1016/bs.irn.2015.05.014.

10. Aryal, P., Dvir, H., Choe, S., and Slesinger, P.A. (2009). A Discrete Alcohol Pocket Involved in GIRK Channel Activation. Nat. Neurosci. *12*, 988–995. 10.1038/nn.2358.

11. Bodhinathan, K., and Slesinger, P.A. (2014). Alcohol modulation of G-protein-gated inwardly rectifying potassium channels: from binding to therapeutics. Front. Physiol. *5*. 10.3389/fphys.2014.00076.

12. Glaaser, I.W., and Slesinger, P.A. (2017). Dual activation of neuronal G protein-gated inwardly rectifying potassium (GIRK) channels by cholesterol and alcohol. Sci. Rep. *7*. 10.1038/s41598-017-04681-x.

13. Blednov, Y.A., Stoffel, M., Chang, S.R., and Adron Harris, R. (2001). GIRK2 deficient mice: Evidence for hyperactivity and reduced anxiety. Physiol. Behav. *74*, 109–117. 10.1016/S0031-9384(01)00555-8.

14. Blednov, Y.A., Stoffel, M., Chang, S.R., and Harris, R.A. (2001). Potassium Channels as Targets for Ethanol: Studies of G-Protein-Coupled Inwardly Rectifying Potassium Channel 2 (GIRK2) Null Mutant Mice. J. Pharmacol. Exp. Ther. *298*, 521–530.

15. Hill, K.G., Alva, H., Blednov, Y.A., and Cunningham, C.L. (2003). Reduced ethanol-induced conditioned taste aversion and conditioned place preference in GIRK2 null mutant mice. Psychopharmacology (Berl.) *169*, 108–114. 10.1007/s00213-003-1472-4.

16. Victoria, N.C., de Velasco, E.M.F., Ostrovskaya, O., Metzger, S., Xia, Z., Kotecki, L., Benneyworth, M.A., Zink, A.N., Martemyanov, K.A., and Wickman, K. (2016). G protein-gated K+ channel ablation in forebrain pyramidal neurons selectively impairs fear learning. Biol. Psychiatry *80*, 796–806. 10.1016/j.biopsych.2015.10.004.

17. Ho, S.-M., Hartley, B.J., Flaherty, E., Rajarajan, P., Abdelaal, R., Obiorah, I., Barretto, N., Muhammad, H., Phatnani, H.P., Akbarian, S., et al. (2017). Evaluating Synthetic Activation and Repression of Neuropsychiatric-Related Genes in hiPSC-Derived NPCs, Neurons, and Astrocytes. Stem Cell Rep. *9*, 615–628. 10.1016/j.stemcr.2017.06.012.

18. Das, S.C., Althobaiti, Y.S., Alshehri, F.S., and Sari, Y. (2016). Binge ethanol withdrawal: Effects on post-withdrawal ethanol intake, glutamate-glutamine cycle and monoamine tissue content in P rat model. Behav. Brain Res. *303*, 120–125. 10.1016/j.bbr.2016.01.052.

19. Kim, K.C., Go, H.S., Bak, H.R., Choi, C.S., Choi, I., Kim, P., Han, S.-H., Han, S.M., Shin, C.Y., and Ko, K.H. (2010). Prenatal exposure of ethanol induces increased glutamatergic neuronal differentiation of neural progenitor cells. J. Biomed. Sci. *17*, 85. 10.1186/1423-0127-17-85.

20. Diana, M., Rossetti, Z.L., and Gessa, G. (1993). Rewarding and aversive effects of ethanol: interplay of GABA, glutamate and dopamine. Alcohol Alcohol. Oxf. Oxfs. Suppl. *2*, 315–319.

21. Läck, A.K., Diaz, M.R., Chappell, A., DuBois, D.W., and McCool, B.A. (2007). Chronic Ethanol and Withdrawal Differentially Modulate Pre- and Postsynaptic Function at Glutamatergic Synapses in Rat Basolateral Amygdala. J. Neurophysiol. *98*, 3185–3196. 10.1152/jn.00189.2007.

22. GTEx Portal https://www.gtexportal.org/home/snp/rs2835872.

23. Ho, S.-M., Hartley, B.J., Tcw, J., Beaumont, M., Stafford, K., Slesinger, P.A., and Brennand, K.J. (2016). Rapid Ngn2-induction of excitatory neurons from hiPSC-derived neural progenitor cells. Methods San Diego Calif *101*, 113–124. 10.1016/j.ymeth.2015.11.019.

24. Savell, K.E., Bach, S.V., Zipperly, M.E., Revanna, J.S., Goska, N.A., Tuscher, J.J., Duke, C.G., Sultan, F.A., Burke, J.N., Williams, D.M., et al. (2018). A neuron-optimized CRISPR/dCas9 activation system for robust and specific gene regulation. bioRxiv, 371500. 10.1101/371500.

25. Loya, A., Pnueli, L., Yosefzon, Y., Wexler, Y., Ziv-Ukelson, M., and Arava, Y. (2008). The 3′-UTR mediates the cellular localization of an mRNA encoding a short plasma membrane protein. RNA *14*, 1352–1365. 10.1261/rna.867208.

26. Tcw, J., Carvalho, C.M.B., Yuan, B., Gu, S., Altheimer, A.N., McCarthy, S., Malhotra, D., Sebat, J., Siegel, A.J., Rudolph, U., et al. (2017). Divergent Levels of Marker Chromosomes in an hiPSC-Based Model of Psychosis. Stem Cell Rep. *8*, 519–528. 10.1016/j.stemcr.2017.01.010.

27. Johnson, M.A., Weick, J.P., Pearce, R.A., and Zhang, S.-C. (2007). Functional neural development from human embryonic stem cells: accelerated synaptic activity via astrocyte coculture. J. Neurosci. Off. J. Soc. Neurosci. *27*, 3069–3077. 10.1523/JNEUROSCI.4562-06.2007.

28. Odawara, A., Saitoh, Y., Alhebshi, A.H., Gotoh, M., and Suzuki, I. (2014). Long-term electrophysiological activity and pharmacological response of a human induced pluripotent stem cell-derived neuron and astrocyte co-culture. Biochem. Biophys. Res. Commun. *443*, 1176–1181. 10.1016/j.bbrc.2013.12.142.

29. Tang, X., Zhou, L., Wagner, A.M., Marchetto, M.C.N., Muotri, A.R., Gage, F.H., and Chen, G. (2013). Astroglial cells regulate the developmental timeline of human neurons differentiated from induced pluripotent stem cells. Stem Cell Res. *11*, 743–757. 10.1016/j.scr.2013.05.002.

30. Federici, M., Nisticò, R., Giustizieri, M., Bernardi, G., and Mercuri, N.B. (2009). Ethanol enhances GABAB-mediated inhibitory postsynaptic transmission on rat midbrain dopaminergic neurons by facilitating GIRK currents. Eur. J. Neurosci. *29*, 1369–1377. 10.1111/j.1460-9568.2009.06700.x.

31. Schreibmayer, W., Dessauer, C.W., Vorobiov, D., Gilman, A.G., Lester, H.A., Davidson, N., and Dascal, N. (1996). Inhibition of an inwardly rectifying K + channel by G-protein α-subunits. Nature *380*, 624. 10.1038/380624a0.

32. Slesinger, P.A., Stoffel, M., Jan, Y.N., and Jan, L.Y. (1997). Defective gamma-aminobutyric acid type B receptor-activated inwardly rectifying K+ currents in cerebellar granule cells isolated from weaver and Girk2 null mutant mice. Proc. Natl. Acad. Sci. U. S. A. *94*, 12210–12217. 10.1073/pnas.94.22.12210.

33. Kuzhikandathil, E.V., and Oxford, G.S. (2002). Classic D1 dopamine receptor antagonist R-(+)-7-chloro-8-hydroxy-3-methyl-1-phenyl-2,3,4,5-tetrahydro-1H-3-benzazepine hydrochloride (SCH23390) directly inhibits G protein-coupled inwardly rectifying potassium channels. Mol. Pharmacol. *62*, 119–126. 10.1124/mol.62.1.119.

34. Zhao, Y., Ung, P.M.-U., Zahoránszky-Kőhalmi, G., Zakharov, A.V., Martinez, N.J., Simeonov, A., Glaaser, I.W., Rai, G., Schlessinger, A., Marugan, J.J., et al. (2020). Identification of a G-Protein-Independent Activator of GIRK Channels. Cell Rep. *31*, 107770. 10.1016/j.celrep.2020.107770.

35. Scarnati, M.S., Boreland, A.J., Joel, M., Hart, R.P., and Pang, Z.P. (2020). Differential sensitivity of human neurons carrying μ opioid receptor (MOR) N40D variants in response to ethanol. Alcohol. 10.1016/j.alcohol.2020.05.004.

36. Lieberman, R., Levine, E.S., Kranzler, H.R., Abreu, C., and Covault, J. (2012). Pilot Study of iPS-derived Neural Cells to Examine Biological Effects of Alcohol on Human Neurons in vitro. Alcohol. Clin. Exp. Res. *36*, 1678–1687. 10.1111/j.1530-0277.2012.01792.x.

37. La Paglia, L., Listì, A., Caruso, S., Amodeo, V., Passiglia, F., Bazan, V., and Fanale, D. (2017). Potential Role of ANGPTL4 in the Cross Talk between Metabolism and Cancer through PPAR Signaling Pathway. PPAR Res. *2017*, e8187235. https://doi.org/10.1155/2017/8187235.

38. Ma, W.-Q., Sun, X.-J., Wang, Y., Zhu, Y., Han, X.-Q., and Liu, N.-F. (2019). Restoring mitochondrial biogenesis with metformin attenuates β-GP-induced phenotypic transformation of VSMCs into an osteogenic phenotype via inhibition of PDK4/oxidative stress-mediated apoptosis. Mol. Cell. Endocrinol. *479*, 39–53. 10.1016/j.mce.2018.08.012.

39. Cippitelli, A., Domi, E., Ubaldi, M., Douglas, J.C., Li, H.W., Demopulos, G., Gaitanaris, G., Roberto, M., Drew, P.D., Kane, C.J.M., et al. (2017). Protection against alcohol-induced neuronal and cognitive damage by the PPARγ receptor agonist pioglitazone. Brain. Behav. Immun. *64*, 320–329. 10.1016/j.bbi.2017.02.001.

40. Jeon, J.-H., Thoudam, T., Choi, E.J., Kim, M.-J., Harris, R.A., and Lee, I.-K. (2020). Loss of metabolic flexibility as a result of overexpression of pyruvate dehydrogenase kinases in muscle, liver and the immune system: Therapeutic targets in metabolic diseases. J. Diabetes Investig. *n/a*. 10.1111/jdi.13345.

41. Zhang, S., Hulver, M.W., McMillan, R.P., Cline, M.A., and Gilbert, E.R. (2014). The pivotal role of pyruvate dehydrogenase kinases in metabolic flexibility. Nutr. Metab. *11*, 10. 10.1186/1743-7075-11-10.

42. Verma, M., Lizama, B.N., and Chu, C.T. (2022). Excitotoxicity, calcium and mitochondria: a triad in synaptic neurodegeneration. Transl. Neurodegener. *11*, 3. 10.1186/s40035-021-00278-7.

43. Cassano, T., Pace, L., Bedse, G., Lavecchia, A.M., De Marco, F., Gaetani, S., and Serviddio, G. (2016). Glutamate and Mitochondria: Two Prominent Players in the Oxidative Stress-Induced Neurodegeneration. Curr. Alzheimer Res. *13*, 185–197. 10.2174/1567205013666151218132725.

44. Giorgi, C., Marchi, S., and Pinton, P. (2018). The machineries, regulation and cellular functions of mitochondrial calcium. Nat. Rev. Mol. Cell Biol. *19*, 713–730. 10.1038/s41580-018-0052-8.

45. Vandecasteele, G., Szabadkai, G., and Rizzuto, R. (2001). Mitochondrial Calcium Homeostasis: Mechanisms and Molecules. IUBMB Life *52*, 213–219. 10.1080/15216540152846028.

46. Sharon, D., Vorobiov, D., and Dascal, N. (1997). Positive and Negative Coupling of the Metabotropic Glutamate Receptors to a G Protein–activated K+ Channel, GIRK, in Xenopus Oocytes. J. Gen. Physiol. *109*, 477–490. 10.1085/jgp.109.4.477.

47. Dutar, P., Petrozzino, J.J., Vu, H.M., Schmidt, M.F., and Perkel, D.J. (2000). Slow Synaptic Inhibition Mediated by Metabotropic Glutamate Receptor Activation of GIRK Channels. J. Neurophysiol. *84*, 2284–2290. 10.1152/jn.2000.84.5.2284.

48. Bocchio, M., Lukacs, I.P., Stacey, R., Plaha, P., Apostolopoulos, V., Livermore, L., Sen, A., Ansorge, O., Gillies, M.J., Somogyi, P., et al. (2019). Group II Metabotropic Glutamate Receptors Mediate Presynaptic Inhibition of Excitatory Transmission in Pyramidal Neurons of the Human Cerebral Cortex. Front. Cell. Neurosci. *12*.

49. Dong, H.-W., and Ennis, M. (2018). Activation of Group II Metabotropic Glutamate Receptors Suppresses Excitability of Mouse Main Olfactory Bulb External Tufted and Mitral Cells. Front. Cell. Neurosci. *11*.

50. Moussawi, K., and Kalivas, P.W. (2010). Group II metabotropic glutamate receptors (mGlu2/3) in drug addiction. Eur. J. Pharmacol. *639*, 115–122. 10.1016/j.ejphar.2010.01.030.

51. Sun, J., Wu, D., Wong, G.C.-N., Lau, M., Yang, M., Hart, R.P., Kwan, K.-M., Chan, E., and Chow, H.-M. (2023). Chronic alcohol metabolism results in DNA repair infidelity and cell cycle-induced senescence in neurons. Aging Cell.

52. Tapia-Rojas, C., Pérez, M.J., Jara, C., and Quintanilla, E.H.V. and R.A. (2017). Ethanol Consumption Affects Neuronal Function: Role of the Mitochondria. Mitochondrial Dis. 10.5772/intechopen.71611.

53. León, B.E., Kang, S., Franca-Solomon, G., Shang, P., and Choi, D.-S. (2022). Alcohol-Induced Neuroinflammatory Response and Mitochondrial Dysfunction on Aging and Alzheimer's Disease. Front. Behav. Neurosci. *15*, 778456. 10.3389/fnbeh.2021.778456.

54. Lim, J.R., Chae, C.W., Park, J.Y., Jung, Y.H., Yoon, J.H., Kim, M.J., Lee, H.J., Choi, G.E., and Han, H.J. (2023). Ethanol-induced ceramide production causes neuronal apoptosis by increasing MCL-1S-mediated ER-mitochondria contacts. Neurobiol. Dis. *177*, 106009. 10.1016/j.nbd.2023.106009.

55. Gunnewiek, T.M.K., Hugte, E.J.H.V., Frega, M., Guardia, G.S., Foreman, K.B., Panneman, D., Mossink, B., Linda, K., Keller, J.M., Schubert, D., et al. (2019). Mitochondrial dysfunction impairs human neuronal development and reduces neuronal network activity and synchronicity. bioRxiv, 720227. 10.1101/720227.

56. Motori, E., Atanassov, I., Kochan, S.M.V., Folz-Donahue, K., Sakthivelu, V., Giavalisco, P., Toni, N., Puyal, J., and Larsson, N.-G. (2020). Neuronal metabolic rewiring promotes resilience to neurodegeneration caused by mitochondrial dysfunction. Sci. Adv. *6*, eaba8271. 10.1126/sciadv.aba8271.

57. Jensen, K.P., Lieberman, R., Kranzler, H.R., Gelernter, J., Clinton, K., and Covault, J. (2019). Alcohol-responsive genes identified in human iPSC-derived neural cultures. Transl. Psychiatry *9*, 96. 10.1038/s41398-019-0426-5.

58. Mathiharan, Y.K., Glaaser, I.W., Zhao, Y., Robertson, M.J., Skiniotis, G., and Slesinger, P.A. (2020). Structural basis of GIRK2 channel modulation by cholesterol and PIP2. bioRxiv, 2020.06.04.134544. 10.1101/2020.06.04.134544.

59. Chung, H.J., Ge, W.-P., Qian, X., Wiser, O., Jan, Y.N., and Jan, L.Y. (2009). G protein-activated inwardly rectifying potassium channels mediate depotentiation of long-term potentiation. Proc. Natl. Acad. Sci. *106*, 635–640. 10.1073/pnas.0811685106.

60. Chung, C.Y., Seo, H., Sonntag, K.C., Brooks, A., Lin, L., and Isacson, O. (2005). Cell type-specific gene expression of midbrain dopaminergic neurons reveals molecules involved in their vulnerability and protection. Hum. Mol. Genet. *14*, 1709–1725. 10.1093/hmg/ddi178.

61. May, L.M., Anggono, V., Gooch, H.M., Jang, S.E., Matusica, D., Kerbler, G.M., Meunier, F.A., Sah, P., and Coulson, E.J. (2017). G-Protein-Coupled Inwardly Rectifying Potassium (GIRK) Channel Activation by the p75 Neurotrophin Receptor Is Required for Amyloid β Toxicity. Front. Neurosci. *11*. 10.3389/fnins.2017.00455.

62. Esposito, Z., Belli, L., Toniolo, S., Sancesario, G., Bianconi, C., and Martorana, A. (2013). Amyloid β, Glutamate, Excitotoxicity in Alzheimer's Disease: Are We on the Right Track? CNS Neurosci. Ther. *19*, 549–555. 10.1111/cns.12095.

63. Velasco, E.M.F. de, Zhang, L., Vo, B., Tipps, M., Farris, S., Xia, Z., Anderson, A., Carlblom, N., Weaver, C.D., Dudek, S.M., et al. (2017). GIRK2 splice variants and neuronal G protein-gated K + channels: implications for channel function and behavior. Sci. Rep. *7*, 1639. 10.1038/s41598-017-01820-2.

64. Topol, A., Zhu, S., Hartley, B.J., English, J., Hauberg, M.E., Readhead, B., Tran, N., Rittenhouse, C.A., Simone, A., Ruderfer, D.M., et al. (2016). Dysregulation of miRNA-9 in a Subset of Schizophrenia Patient-Derived Neural Progenitor Cells. Cell Rep. *15*, 1024–1036. 10.1016/j.celrep.2016.03.090.

65. Halikere, A., Popova, D., Scarnati, M.S., Hamod, A., Swerdel, M.R., Moore, J.C., Tischfield, J.A., Hart, R.P., and Pang, Z.P. (2020). Addiction associated N40D mu-opioid receptor variant modulates synaptic function in human neurons. Mol. Psychiatry *25*, 1406–1419. 10.1038/s41380-019-0507-0.

66. Schindelin, J., Arganda-Carreras, I., Frise, E., Kaynig, V., Longair, M., Pietzsch, T., Preibisch, S., Rueden, C., Saalfeld, S., Schmid, B., et al. (2012). Fiji: an open-source platform for biological-image analysis. Nat. Methods *9*, 676–682. 10.1038/nmeth.2019.

67. Yang, N., Chanda, S., Marro, S., Ng, Y.-H., Janas, J.A., Haag, D., Ang, C.E., Tang, Y., Flores, Q., Mall, M., et al. (2017). Generation of pure GABAergic neurons by transcription factor programming. Nat. Methods. 10.1038/nmeth.4291.

68. Zhang, Z.-M., Chen, S., and Liang, Y.-Z. (2010). Baseline correction using adaptive iteratively reweighted penalized least squares. The Analyst *135*, 1138–1146. 10.1039/b922045c.

69. Ligges, U., Short, T., Kniezle, P., Schnackenberg, S., Billinghurst, D., Borchers, H.-W., Carezia, A., Dupuis, P., Eaton, J.W., Farhi, E., et al. (2021). signal: Signal Processing.

70. Borchers, H.W. (2022). pracma: Practical Numerical Math Functions.

71. R Core Team (2020). R: A Language and Environment for Statistical Computing.

72. Long, J.A. (2022). jtools: Analysis and Presentation of Social Scientific Data.

73. Bates, D., Maechler, M., Bolker [aut, B., cre, Walker, S., Christensen, R.H.B., Singmann, H., Dai, B., Scheipl, F., Grothendieck, G., et al. (2022). lme4: Linear Mixed-Effects Models using "Eigen" and S4.

74. Wickham, H., Chang, W., Henry, L., Pedersen, T.L., Takahashi, K., Wilke, C., Woo, K., Yutani, H., Dunnington, D., and RStudio (2023). ggplot2: Create Elegant Data Visualisations Using the Grammar of Graphics.